iScience

CellPress
OPEN ACCESS

Article

Resolving macrophage polarization through distinct Ca^{2+} entry channel that maintains intracellular signaling and mitochondrial bioenergetics

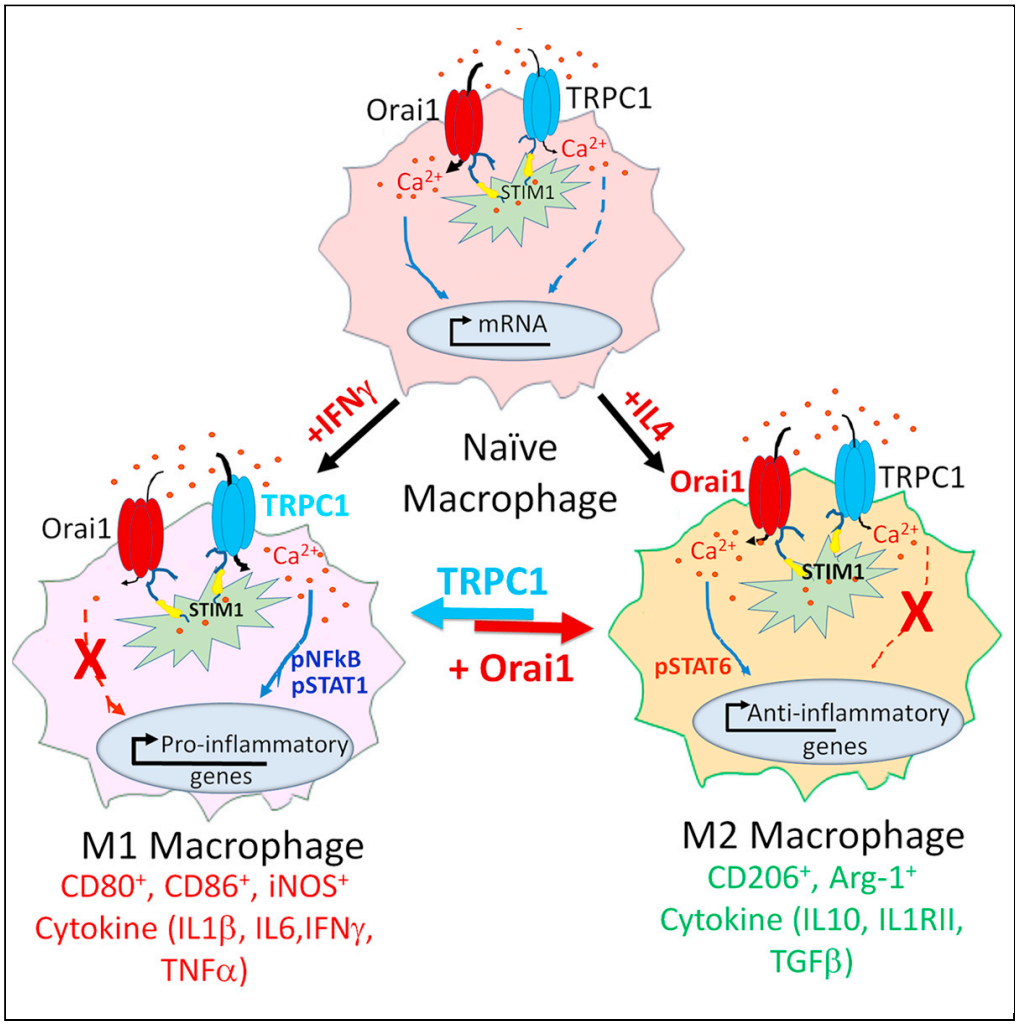

Viviane Nascimento Da Conceicao, Yuyang Sun, Karthik Ramachandran, ..., Bibhuti B. Mishra, Muniswamy Madesh, Brij B. Singh

singhbb@uthscsa.edu (B.B.S.)
muniswamy@uthscsa.edu (M.M.)
bibhuti.mishra@med.und.edu (B.B.M.)

Highlights

Store-operated Ca^{2+} entry is essential for macrophage activation and function

Orai1 activation of STAT6 dictates the anti-inflammatory M2 phenotype

TRPC1-mediated activation of pNF-κB/ STAT1 is critical for M1 phenotype

Alteration in TRPC1/Orai1 expression transforms M1/M2 polarization

Nascimento Da Conceicao et al., iScience 24, 103339 November 19, 2021
https://doi.org/10.1016/j.isci.2021.103339

iScience

CellPress
OPEN ACCESS

Article

Resolving macrophage polarization through distinct Ca^{2+} entry channel that maintains intracellular signaling and mitochondrial bioenergetics

Viviane Nascimento Da Conceicao,[1] Yuyang Sun,[1] Karthik Ramachandran,[2] Arun Chauhan,[3] Amritha Raveendran,[3] Manigandan Venkatesan,[2] Bony DeKumar,[3] Soumya Maity,[2] Neelanjan Vishnu,[2] George A. Kotsakis,[1] Paul F. Worley,[4] Donald L. Gill,[5] Bibhuti B. Mishra,[3,*] Muniswamy Madesh,[2,*] and Brij B. Singh[1,6,*]

SUMMARY

Transformation of naive macrophages into classically (M1) or alternatively (M2) activated macrophages regulates the inflammatory response. Here, we identified that distinct Ca^{2+} entry channels determine the IFNγ-induced M1 or IL-4-induced M2 transition. Naive or M2 macrophages exhibit a robust Ca^{2+} entry that was dependent on Orai1 channels, whereas the M1 phenotype showed a non-selective TRPC1 current. Blockade of Ca^{2+} entry suppresses pNF-κB/pJNK/STAT1 or STAT6 signaling events and consequently lowers cytokine production that is essential for M1 or M2 functions. Of importance, LPS stimulation shifted M2 cells from Orai1 toward TRPC1-mediated Ca^{2+} entry and $TRPC1^{-/-}$ mice exhibited transcriptional changes that suppress pro-inflammatory cytokines. In contrast, $Orai1^{-/-}$ macrophages showed a decrease in anti-inflammatory cytokines and exhibited a suppression of mitochondrial oxygen consumption rate and inhibited mitochondrial shape transition specifically in the M2 cells. Finally, alterations in TRPC1 or Orai1 expression determine macrophage polarization suggesting a distinct role of Ca^{2+} channels in modulating macrophage transformation.

INTRODUCTION

Macrophages are essential for the innate immunity where they eliminate pathogens either directly via phagocytosis or by the production of cytokines that elicits adaptive immune response (Benoit et al., 2008). Cytokines such as interferon (IFNγ) transform resting macrophages into classically activated macrophages, commonly known as the M1 phenotype. M1 macrophages amplify the cellular antigen presenting capacity, complement mediated phagocytosis, and secrete pro-inflammatory cytokines, such as tumor necrosis factor (TNF)-α, interleukin (IL-1, 6), STAT1, STAT3, IRF4, NF-κB, CIITA, CD80, CD86, and reactive nitrogen, which leads to a strong bactericidal and tumoricidal activity (Brodsky, 2020; Feske et al., 2015; Han et al., 2017). Similarly, IL-4, which is mainly produced by Th2 cells, transforms naive macrophages into alternatively activated macrophages, or the M2 phenotype, which express molecules including Arginase1 (Arg1), chitinase 3, OCS1, PPARγ, STAT6, GATA3, c-MYC, HIF-1α, LXR, CD163, CD36, TGFβ, IL-10, and CD206. These molecules are associated with parasitic infestations and promote tissue remodeling (Cairo et al., 2011; Jha et al., 2015; Viola et al., 2019). Although macrophage transition is stimulus specific, the exact mechanism(s) is not fully known. Of importance, Ca^{2+} homeostasis has been shown to be essential for cytokine production and its release and thus could contribute toward macrophage plasticity.

Increase in intracellular Ca^{2+} ($[Ca^{2+}]_i$) levels regulates cytokine production and plays a central role in macrophage function. In macrophage cells, release of Ca^{2+} from the internal endoplasmic reticulum (ER) stores leads to the activation of the store operated Ca^{2+} entry (SOCE) mechanism (Clapham, 2007; Li et al., 2011; Parekh and Putney, 2005). Similarly, agonist binding to the cell surface receptors generates second messenger (IP_3) that induces the release of Ca^{2+} from the ER. Once ER Ca^{2+} stores are depleted, Stromal Interaction Molecule 1 (STIM1), which acts as an ER Ca^{2+} sensor, aggregates and activates the plasma membrane Ca^{2+} influx channels. Two distinct Ca^{2+} influx channels, Ca^{2+} release-activated Ca^{2+} channel (Orai1) (Bollimuntha et al., 2011; Feske et al., 2006; Liao et al., 2008; Zhou et al., 2016) and Transient

[1]Department of Periodontics, University of Texas Health San Antonio, San Antonio, TX 78229, USA

[2]Department of Medicine, Cardiology Division, Center for Precision Medicine, University of Texas Health San Antonio, San Antonio, TX 78229, USA

[3]Department of Biomedical Sciences, School of Medicine and Health Sciences, University of North Dakota, Grand Forks, ND 58202, USA

[4]Department of Neuroscience, Johns Hopkins University School of Medicine, Baltimore, MD 21205, USA

[5]Department of Cellular and Molecular Physiology, Penn State Hershey College of Medicine, Hershey, PA 17033, USA

[6]Lead contact

*Correspondence: singhbb@uthscsa.edu (B.B.S.), muniswamy@uthscsa.edu (M.M.), bibhuti.mishra@med.und.edu (B.B.M.)

https://doi.org/10.1016/j.isci.2021.103339

Receptor Potential Canonical 1 (TRPC1) channel, have been shown to interact with STIM1 to raise $[Ca^{2+}]_i$ (Chauhan et al., 2018; Ong et al., 2016). Loss of Orai1 or STIM1 leads to an impaired immune function in lymphocytes (Feske et al., 2006), but the precise role of different Ca^{2+} entry channels in macrophage phenotypes is not known. Therefore, identifying the identity of the Ca^{2+} entry channels and establishing the mechanism(s) by which they induce immune activation/resolution is critical for understanding the innate immune response.

Non-cytokine pathways such as hypoxia and the production of lactate due to inhibition of mitochondrial function are also shown to induce macrophage transition (Viola et al., 2019). Metabolic rewiring has been suggested to contribute toward macrophages plasticity; however, factors that modulate metabolic changes are not known. In addition, changes in gene and protein expression also contribute to immune function. In response to their microenvironment, macrophages adapt their phenotype mainly through regulating transcription, which depends on the stimuli they encounter. In addition, triggering Ca^{2+} fluxes have been shown to be an essential component of the epigenetic changes that regulate gene expression and alter metabolic profiles (Gautier et al., 2012; Murray et al., 2014). Moreover, epigenetic modulators have been shown to alter Ca^{2+} homeostasis (Izquierdo-Torres et al., 2020; Pagiatakis et al., 2019; Raynal et al., 2016), suggesting that Ca^{2+} channels could play a critical role in modulating gene expression essential for immune activation and its resolution. The aim of this study was to identify and characterize the Ca^{2+} channels present in various macrophage subtypes. Our data provide evidence that Ca^{2+} homeostasis in naive and M2 macrophages is driven by Orai1 channels, whereas the M1 phenotype is strictly dependent on TRPC1-activated STAT1/NF-κB pathway. We also report for the first time that dysfunction in Ca^{2+} channel expression prevents IFNγ or IL-4-mediated transition of M1 to M2 macrophage phenotype. Together, these results suggest that elevated TRPC1-mediated Ca^{2+} signaling leads to M1 function, whereas Orai1-mediated Ca^{2+} signaling modulates the M2 macrophage phenotype. Moreover, Ca^{2+} entry-mediated phenotypic changes are partly through mitochondrial shape transition and bioenergetics.

RESULTS

Characterization of store-operated Ca^{2+} channels in naive bone marrow-derived macrophages

Naive primary macrophage cells were isolated from mice bone marrow, and cells that were F4/80 and CD11b positive were used for all experiments (Figure 1A). To address whether blocking Ca^{2+} entry channels has an impact on naive macrophages (Mφ) proliferation, we used known Ca^{2+} entry inhibitors 2APB and SKF96365 (+SKF) (Waldron et al., 1997). A significant decrease in cell proliferation and cell viability was observed when naive Mφ cells were incubated with these inhibitors (Figures 1B and S1A). Addition of thapsigargin (Tg) (1 μM in Ca^{2+}-free buffer), which is a known SERCA pump blocker, led to the depletion of ER Ca^{2+} as observed by an increase in intracellular Ca^{2+} ($[Ca^{2+}]_i$) levels (first peak) (Figures 1B and 1C). The addition of 1 mM external Ca^{2+} showed a significant elevation in $[Ca^{2+}]_i$ (second peak), indicating the presence of SOCE in these cells (Figures 1C and 1D). Moreover, cells treated with SKF-96365 or 2APB showed a significant reduction in both ER Ca^{2+} levels and SOCE (Figures 1C, 1D, S1B, and S1C). To establish the molecular identity of the Ca^{2+} influx channel in naive Mφ cells, electrophysiological recordings of the membrane currents were performed. Addition of Tg induced a Ca^{2+} current, which was partially inward rectifying (Figures 1E and 1F). The whole-cell currents in naive Mφ cells developed before the application of thapsigargin (due to high BAPTA in the patch pipette), and the current observed was partially inward rectifying. Although the current properties observed here were slightly similar as has been reported with Orai1 channels (Feske et al., 2006; Liao et al., 2008; Sukumaran et al., 2016; Zhou et al., 2016), they still showed some outward currents, suggesting that this could still be a mixed current. Consistent with these results, addition of SKF-96365 (nonspecific Ca^{2+} channel blocker) or Synta66 (Orai1 inhibitor) (Table S1 related to STAR Methods) was able to significantly inhibit the Tg-induced Ca^{2+} currents (Figures 1E–1G), suggesting that Orai1 could be the major Ca^{2+} entry channel in naive Mφ cells.

We next studied the role of bacterial lipopolysaccharide (LPS) that is known to induce the M1 phenotype. Naive Mφ cells treated with LPS (100 ng/mL for 6 h) showed an increase in $[Ca^{2+}]_i$, which was again inhibited by the addition of SKF-96365 or 2APB (Figures 1H and 1I). Immunoblot analysis of the Ca^{2+} entry channels showed an increase in TRPC1 expression, whereas no significant change in Orai1 or STIM1 expression was observed upon LPS treatment (Figures 1J and S1D). Of interest, the current properties were also different in LPS-treated cells as a more linear (outward rectifying) TRPC1-like Ca^{2+} current was observed, which was still blocked by SKF-96365 or 2APB (Figures 1K and 1L) (Liu et al., 2017; Selvaraj et al., 2012). To further establish

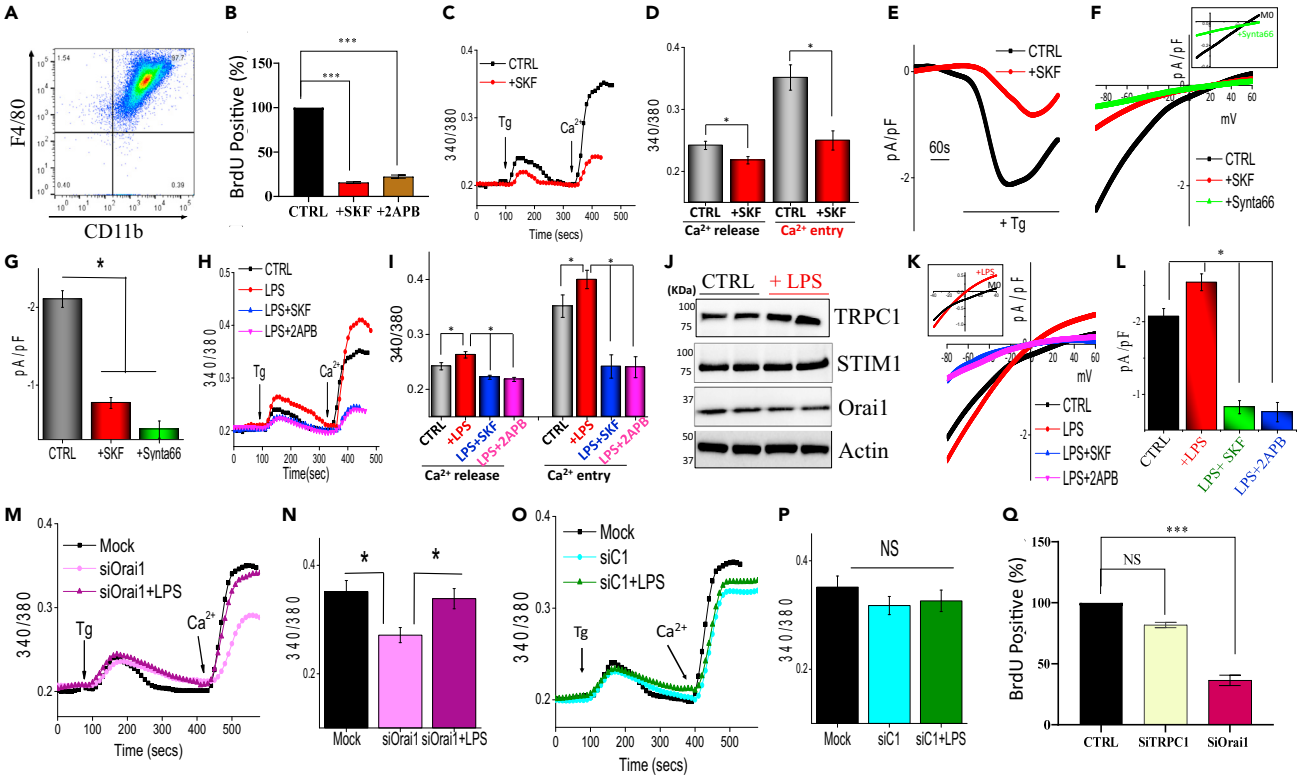

Figure 1. Orai1 expression is essential to development and proliferation of *in vitro* bone marrow-derived naive macrophage from wild-type (WT) mice (C57BL/6J)

(A) Naive Mφ (M0) cells from WT mice (C57BL/6J) were generated using L929 supplemented media. Analysis was performed using flow cytometer, and the levels of F4/80+ CD11b+ were used to show efficacy of cell maturation (Mφ). n = 4 independent experiments with replicates.

(B) Cell proliferation (using BrdU colorimetric assays) was evaluated in naive Mφ (M0) from WT mice cells cultured in the presence or absence of 10 μM SKF96365 or 50 μM 2APB. Data shown are representative of three independent experiments with two replicates. Bar graphs depict average ±SD for BrdU-positive cells, ***$p \leq 0.001$ (Student's t test).

(C) Representative Ca^{2+} trace (from 110 to 160 cells imaged from three separate experiments) showing Thapsigargin (Tg)-evoked ER Ca^{2+} depletion followed by extracellular Ca^{2+}-induced $[Ca^{2+}]_i$ entry in Mφ cells pretreated with and without 50 μM SKF96365 for 6 h.

(D) Bar graphs depict average ± SEM of the fluorescence ratio (340/380) from an average of 110–160 cells. *$p \leq 0.05$ (Student's t test).

(E–G) Application of 2 μM Thapsigargin (Tg) in bath solution induced calcium currents at −80 mV in control and 50 μM SKF96365-treated Mφ cells. Respective IV curves (F) of the currents (leak/background subtracted) and quantitation (8–10 individual recordings) of the current intensity at −80 mV are shown in (G). *$p \leq 0.05$ (Student's t test).

(H) Representative trace showing Thapsigargin (Tg)-evoked Ca^{2+} entry in naive Mφ cells pretreated with and without LPS, LPS +10 μM SKF96365 for 6 h, and LPS+50 μM of 2APB. n = 3–5 independent replicates for each experiment performed in duplicate.

(I) Bar graphs depict average ± SEM, *$p \leq 0.05$ (Student's t test) in individual conditions as labeled.

(J) Immunoblotting analysis showing expression of TRPC1, STIM1, Orai1, and β-actin in naive Mφ from WT mice cultured in the presence or absence of LPS treatment (100 ng/mL for 6 h). n = 3 independent experiments performed in duplicate.

(K and L) IV curves of SOCE currents under various conditions and quantitation (6–8 recordings for each condition) of current intensity at −80 mV is shown in L. *$p \leq 0.05$.

(M) Representative traces showing calcium entry in control and Orai1-silenced (siOrai1) naive Mφ cells, with and without LPS treatment (100 ng/mL for 6 h). n = 3–5 independent replicates.

(N) Average data ± SEM from 90 to 120 cells is provided as bar diagram, *$p \leq 0.05$ (Student's t test).

(O) Thapsigargin (Tg) evoked Ca^{2+} entry in TRPC1-silenced (siC1) naive Mφ cells, in the presence or absence of LPS treatment (100 ng/mL for 6 h). n = 3 to 4 separate experiments.

(P) Bar diagram of the fluorescence ratio (340/380) from an average of ~100 cells in each condition. Bar graphs depict average ± SEM, NS, non-significant.

(Q) Cell proliferation assay was performed in cells from WT mice treated with siControl (CTRL), siTRPC1, or siOrai1 cells. Data shown are representative of three independent experiments with similar results. Bar graphs depict average ± SE for positive cells in four separate experiments, NS, non-significant, ***$p \leq 0.001$ (Student's t test).

the functional role of Orai1/TRPC1 channels in naive Mφ, cells were transfected with either siOrai1 or siTRPC1 with and without LPS stimulation. siOrai1 Mφ cells showed a decrease in Orai1 expression (only the long form of Orai1 is observed in these cells) along with a decrease in Ca^{2+} influx (Figures 1M, 1N,

and S1F–S1G); however, addition of LPS was able to further increase Ca^{2+} entry (Figures 1M and 1N). In contrast, naive Mφ cells transfected with siTRPC1 displayed no significant decrease in Tg-induced Ca^{2+} influx and increase in LPS-stimulated Ca^{2+} entry was also inhibited (Figures 1O, 1P, and S1I–S1L). To further ascertain the influence of TRPC1 and Orai1 on naive Mφ cells, proliferation and cell viability were evaluated. A considerable decrease in both cell proliferation and cell viability was observed in the absence of Orai1, as compared with the loss of TRPC1 or control siRNA (Figures 1Q and S1M). Together, these results suggest that the Ca^{2+} entry channel in naive Mφ cells is dependent on Orai1; however, LPS stimulation significantly alters the properties of the Ca^{2+} currents and non-specific TRPC1-like currents were induced.

Distinct Ca^{2+} entry channel properties are present in M1 and M2 phenotypes

In the next set of experiments, we evaluated the identity of the Ca^{2+} channels in polarized Mφ cells. As described in Figure 2A we induced M1 and M2 phenotypes using IFNγ (20 ng/mL for 24 h) and IL4 (20 ng/mL for 24 h), respectively. Flow cytometry was used to confirm macrophage polarization by measuring specific markers known to be activated by each phenotype: CD80, CD86, and iNOS for M1 and CD206 and Arginase1 for M2 (Figures S2A and B). Of importance, phagocytosis, which is a key function of M1, or angiogenesis, which is a function of M2, was significantly decreased upon addition of SKF-96365 (Figures S2C–S2E). Similarly, flow cytometry analysis on M1 and M2 cells also showed that macrophage transition was dependent on Ca^{2+} channel inhibitor BTP2 (Figures S2F–S2I). These results further emphasize the role of Ca^{2+} entry channels; however, the molecular identity of the channel in M1 and M2 cells is not yet established. Thus, to characterize Ca^{2+} signaling, Ca^{2+} entry was observed by the addition of Tg, followed by the addition of extracellular Ca^{2+}. It was observed that both ER Ca^{2+} and Ca^{2+} entry were significantly higher in the M1 phenotype as compared with the control naive Mφ cells (Figures 2B and 2C). The current properties in M1 cells mimicked liner non-inward rectifying TRPC1-like currents (Figures 2D–2F). Addition of LPS (100 ng/mL for 6 h) did not further potentiate Ca^{2+} entry, whereas silencing of TRPC1 (+siTRPC1) decreased these currents in M1 cells (Figures 2D–2F). The M2 phenotype also showed an increase in Tg-mediated ER Ca^{2+} release and Ca^{2+} entry but maintained the partially inward rectifying Orai1-like currents that were observed in naive Mφ cells (Figures 2G–2K). On the other hand, LPS treatment not only increased Ca^{2+} entry in M2 cells, but the properties of the Ca^{2+} current started to shift (reversal at 0 mV) and increasing outward currents (that mimics TRPC1-like currents) were observed (Figures 2J and 2K).

To further delineate the reason for elevated plasma membrane Ca^{2+} entry, gene expression analysis was performed on IFNγ and IL-4 treated naive Mφ cells. Curiously, IFNγ, but not IL-4, treatment showed a time-dependent increase in TRPC1 mRNA levels, whereas IL-4 treatment significantly raised Orai1 mRNA levels (Figure 2L). These results complemented protein expression data where we observed an increase in TRPC1 expression upon IFNγ treatment and addition of IL-4 increased the Orai1 expression (Figures 2M and S2J). Expression of TRPC1 was significantly increased in M2 cells that were treated with LPS, along with a decrease in Orai1 levels (Figures S2K and L). In addition, the levels of proinflammatory cytokines (IL-6 and IFNγ) were also increased in M2 cells after LPS treatment along with a decrease in anti-inflammatory cytokines (IL-10 and IL-1RII) (Figure 2N). M1 macrophages failed to be potentiated by LPS, and no further increase in the activation of classical M1 markers (iNOS, CD80, and CD86) was observed in these cells (Figures S2M and N). In contrast, activated M2 cells showed a significant increase in the expression of M1 markers, along with a decrease in the M2 markers, when treated with LPS (Figures S2O and P). Together, these results suggest that distinct Ca^{2+} entry channels are necessary for maintaining both the M1 and M2 phenotypes, and the M1 phenotype is probably mediated through TRPC1, whereas the M2 phenotype is probably dependent on Orai1.

M1 phenotype is mediated via TRPC1-dependent activation of STAT1/NF-κB pathway, whereas M2 phenotype depends on Orai1-mediated activation of STAT6

To delineate the downstream signaling mechanism(s) in M1 and M2 cells, which are induced by these Ca^{2+} influx channels, we next investigated the transcription factors involved in these individual phenotypes. As expected, proinflammatory (for M1) and anti-inflammatory (for M2) cytokines were significantly decreased after SKF-96365 treatment, when compared with control untreated cells (Figures 3A and 3B). Flow cytometry further showed that addition of SKF-96365 decreased both the surface and internal markers for M1 (CD80 and iNOS) and M2 (CD206 and Arginase 1) phenotypes (Figures 3C and 3D). Moreover, a significant reduction in pNF-κB and pJNK levels was observed in M1 cells that were treated with SKF-96365 (Figures 3E; S3A, and S3B). Similarly, arginase1, which is critical for the M2 phenotype, showed a significant decrease in its expression along with a decrease in STAT6 phosphorylation in SKF-96365-treated M2 cells

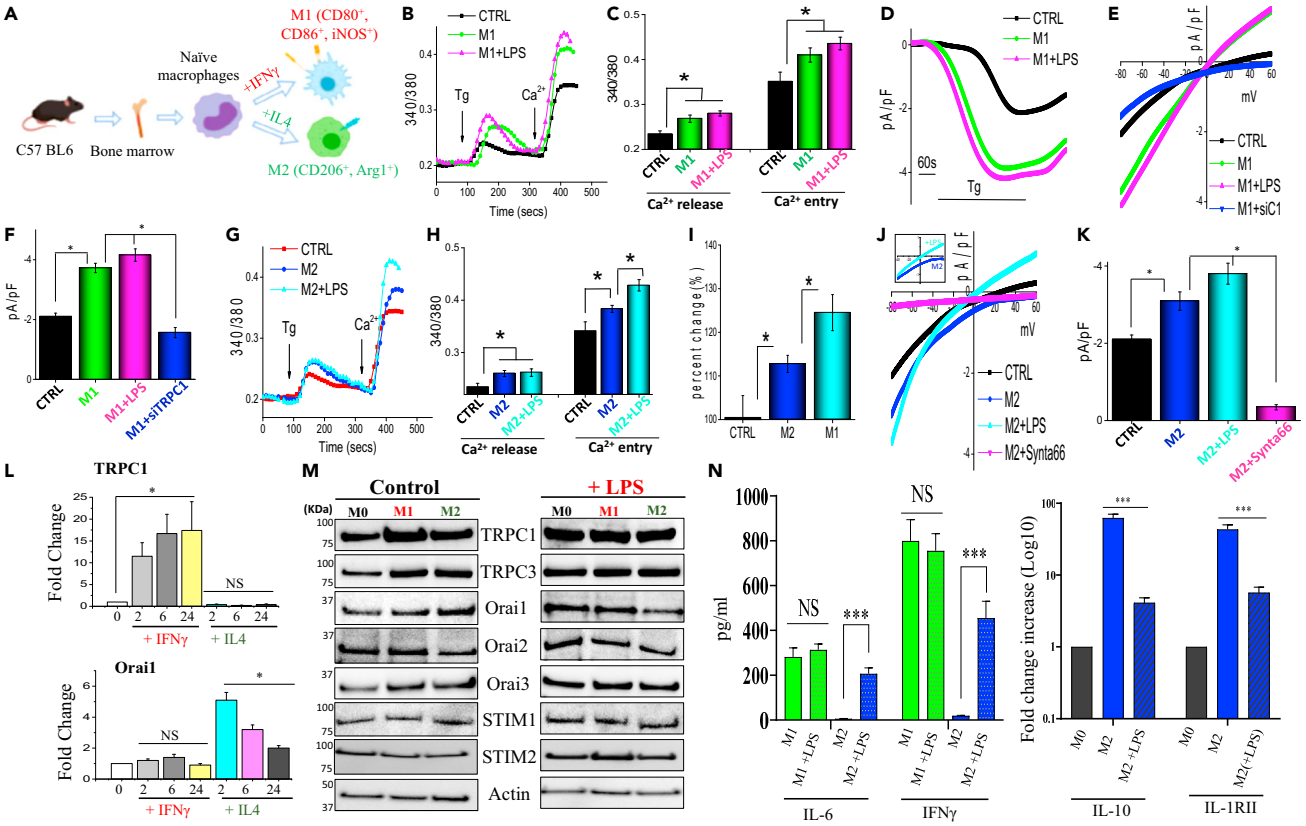

Figure 2. TRPC1 and Orai1 Ca^{2+} currents are observed with IFNγ and IL4-mediated polarization

(A) Schematic overview of macrophage polarization from bone marrow of WT mice. Cells obtained from bone marrow are cultured for 7 days in media containing L929 followed by (IFNγ [20 ng/mL] for M1 and IL4 [20 ng/mL] for M2 macrophages) stimulation.

(B) Ca^{2+} imaging was performed in M1 cells from WT mice. Representative trace showing Thapsigargin (Tg)-evoked Ca^{2+} release and entry in various cells as labeled. LPS (100 ng/mL for 6 h) was added in the media.

(C) Bar diagram of the fluorescence ratio (340/380) from an average of 85 to 140 cells imaged. Bar graphs depict average ± SEM, *p ≤ 0.05 (Student's t test).

(D–F) Application of 2 μM Thapsigargin (Tg, in bath solution) induced inward currents at -80 mV in control naive Mφ, M1, and 100 ng/mL LPS-treated (for 6 h) M1 cells. Respective IV curves of currents and quantitation (8–16 recordings for each condition) of current intensity at −80 mV is shown in (E and F). *p ≤ 0.05 (Student's t test).

(G) Representative trace showing Thapsigargin (Tg)-evoked Ca^{2+} entry in naive, M2, M2+LPS (100 ng/mL for 6 h). Data shown are representative of three independent experiments imaging 50–80 cells for each condition.

(H and I) Bar diagram of the fluorescence ratio (340/380) from an average of 50–80 cells. Bar graphs depict average ± SEM, *p ≤ 0.01 (Student's t test). Similarly, percent change in cytosolic Ca^{2+} levels in various stimulation are shown as bar graph in (I) *p ≤ 0.01 (Student's t test). Data shown are representative of three independent experiments with similar results.

(J and K) IV curves of SOCE currents under various conditions and quantitation (5–8 recordings) of current intensity at −80 mV is shown in (J) *p ≤ 0.05 (Student's t test). Data shown are representative of 5–8 independent experiments with similar results.

(L) Real-time PCR analysis to evaluate TRPC1 and Orai1 expression. mRNA level was normalized using 18S RNA, and fold change in mRNA expression of TRPC1 and Orai1 after each treatment is expressed as arbitrary units. Data shown are representative of two independent experiments performed in triplicates. Significant differences were measured by Student's t test (*p < 0.001; NS, significance).

(M) Immunoblot analysis showing protein level in naive (M0), M1, and M2 macrophages from WT mice with and without LPS (100 ng/mL for 6 h). Data shown are representative of three independent experiments with similar results.

(N) Naive M0, M1, and M2 cells were treated from WT mice cultured in 6-well plate (2×10^6 cells/well) and treated with or without LPS (100 ng/mL) for 6 h. The concentration of pro-inflammatory (IL-6 and IFNγ) and anti-inflammatory (IL1-0 and IL-1RII) cytokines released in the media was performed by ELISA. Data shown are representative of three independent experiments with similar results. Bar graphs depict average ± SD for relative values, ***p ≤ 0.001, NS, non-significant (Student's t test).

(Figures 3F, S3A, and S3B). As TRPC1 expression was increased in the M1 phenotype, we next performed chromatin immunoprecipitation assays to identify the upstream transcription factors responsible for increasing TRPC1 expression. An increase in pNF-κB and pJNK binding to the TRPC1 promoter was observed upon IFNγ treatment but not in the presence of IL-4 (Figures 3G and 3H). In contrast, pSTAT6

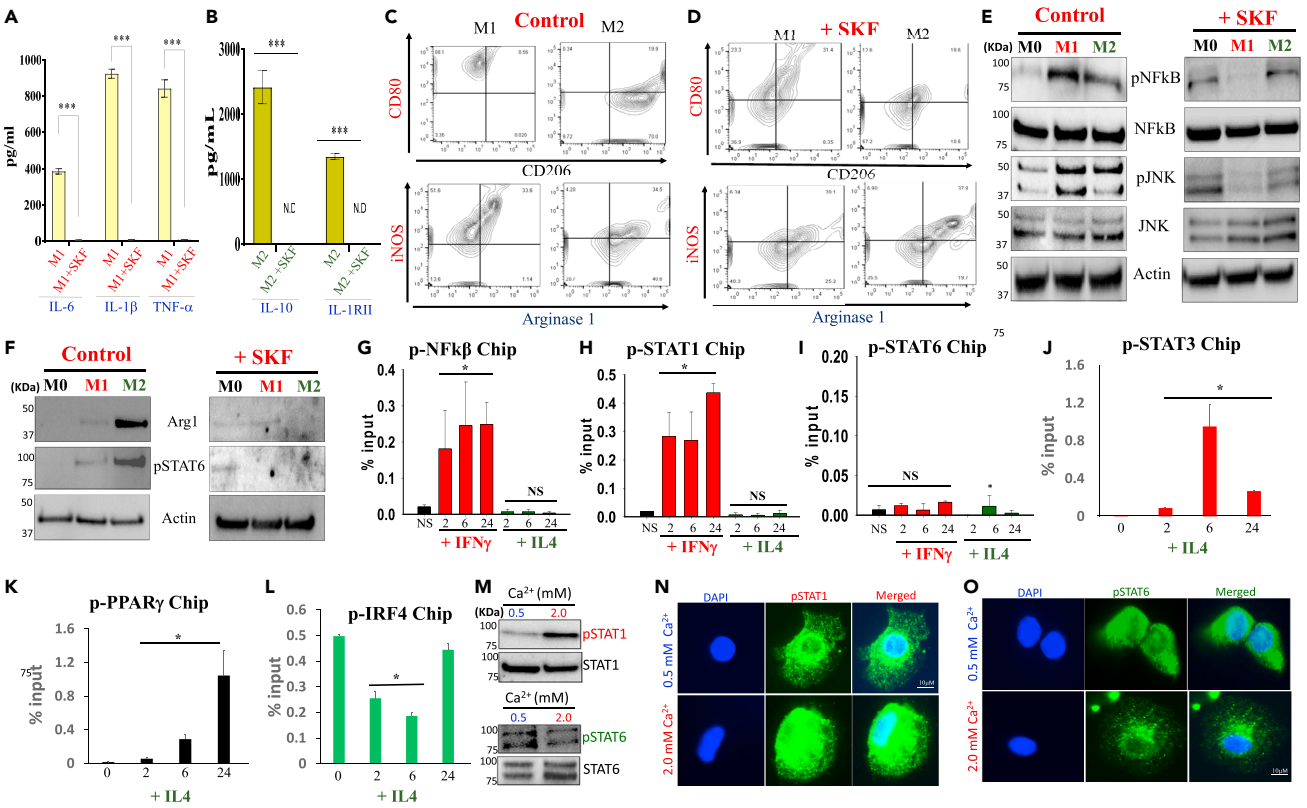

Figure 3. Macrophage polarization is dependent on SOCE channels, and inhibition of these channels disrupts cytokine release

(A and B) Cytokine analysis by colorimetric analysis in supernatants of M1 and M2 activated bone marrow-derived macrophage (BMDM) from wild type after treatment with and without SKF96365 (10 μM for 6 h). Data shown are representative of three independent experiments performed in triplicates. Bar graphs depict average ± SD for relative values, ***p ≤ 0.001 (Student's t test).

(C and D) Flow cytometer analysis on M1 and M2 activated wild-type mice BMDM with and without SKF96365 (10 μM for 6 h) to show how Ca^{2+} inhibition interrupts macrophage polarization by blocking surface (CD80 + CD206+) and internal (iNOS and Arginase-1) markers for the different phenotypes. Data shown are representative of three independent experiments.

(E) Immunoblot analysis showing the level of expression of wild-type mice M1 activated BMDM pathway genes pNF-κB, NF-κB, pJNK, JNK in media treated for 6 h with SKF96365 (10 μM). Data shown are representative of three independent experiments with similar results.

(F) Immunoblot analysis showing the level of expression of wild-type mice M2 activated BMDM pathway genes Arg1, pSTAT6 in media treated for 6 h with SKF96365 (10 μM). Data shown are representative of three independent experiments.

(G–I) Primary macrophages derived from bone marrow were pulsed with medium alone (NS), IFNγ at 20 ng/mL, IL4 at 20 ng/mL, and cultured for a total of 2, 6, and 24-h period. Cells were harvested and chromatin immunoprecipitation (ChIP) experiments was performed with anti-pNF-κB, anti-pSTAT1, or anti-pSTAT6 at the promoter regions of TRPC1 was assessed by qPCR and expressed as percentage of input. The mean ± SE of NF-κB (G), pSTAT1 (H), pSTAT6 (I) are shown.

(J–L) Time-dependent binding to Orai1 promoter region by pSTAT3, pPPARg, and pIRF4 upon IL-4 stimulation; data presented are mean ± SE for each condition. Significant differences were measured by Student's t test (*p < 0.05; NS, non-significant, n = 3).

(M–O) Immunoblot analysis showing the level of expression of phosphorylated STAT1 and STAT6 in M1 and M2 cells that were treated for 24 h in 0.5 or 2 mM external calcium. Data shown are representative of three independent experiments. Representative confocal images showing localization of pSTAT1(N) and pSTAT6(O) in cytoplasm and in the nucleus (co-localization with DAPi staining) in cells treated with various calcium concentrations. Scale bar, 10 μm.

or control IgG antibodies failed to show any binding with the TRPC1 promoter region (Figures 3I and S3C). To evaluate how Orai1 expression is increased in M2 cells, chromatin immunoprecipitation assays were performed, which identified an increase in pSTAT3/6 and pPPARγ, but not pIRF4, binding to the Orai1 promoter upon IL-4 treatment (Figures 3J–L), suggesting that increase in TRPC1 and Orai1 expression is mediated through different transcriptional factors that are dictated by IFNγ or IL-4 signaling.

To further understand as to how Ca^{2+} entry could dictate these opposing events, we altered extracellular Ca^{2+} levels as previous studies have shown that Ca^{2+} has a differential effect on various transcription factors (Kar and Parekh, 2015; Lin et al., 2019). Of importance, increase in extracellular Ca^{2+} (2 mM) further increased STAT1 phosphorylation, as well as pSTAT1 migration into the nucleus was increased (Figures 3M and 3N). In contrast, increase in extracellular Ca^{2+} decreased the phosphorylation of STAT6, as well

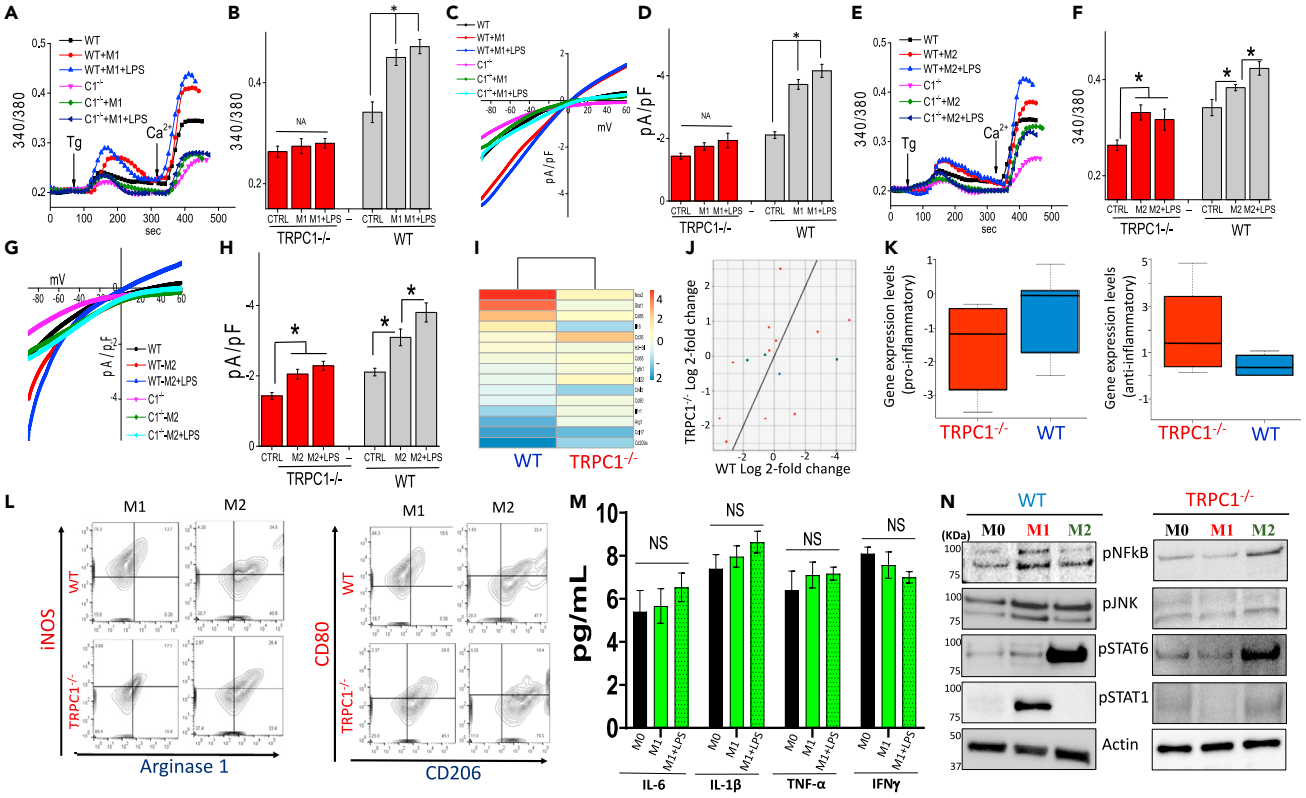

Figure 4. TRPC1$^{-/-}$ mice show no M1 phenotype development even upon LPS treatment

(A) Ca^{2+} imaging performed on M1 cells from control (WT) and TRPC1$^{-/-}$ mice. Representative trace showing Thapsigargin (Tg)-evoked $[Ca^{2+}]_i$ changes in naive and M1 cells pretreated with and without LPS (100 ng/mL) treatment for 6 h. Data shown are representative of three independent experiments with 110–140 cells each.

(B) Bar diagram showing quantification of the fluorescence ratio (340/380) from an average of ~100 cells are shown underneath the traces. Bar graphs depict average ± SEM (Student's t test). Data shown are representative of three independent experiments with similar results.

(C and D) Application of 2 μM Thapsigargin (Tg) in bath solution induced inward currents at −80 mV in control and LPS (100 ng/mL)-treated M1 cells. Respective IV curves of currents and quantitation (8–10 recordings) of current intensity at −80 mV are shown in (C). Bar graphs depict average ± SEM (Student's t test). Data shown are representative of three independent experiments with similar results.

(E) Ca^{2+} imaging performed in M2 cells from control (WT) and TRPC1$^{-/-}$ mice. Representative trace showing Thapsigargin (Tg)-evoked $[Ca^{2+}]_i$ changes in naive and M2 treated cells upon pretreatment with and without LPS (100 ng/mL) for 6 h. Data shown are representative of three independent experiments with similar results.

(F) Bar diagram showing quantification of the fluorescence ratio (340/380) from an average of 90–120 cells are shown underneath the traces. Bar graphs depict average ±SEM, *p ≤ 0.05 (Student's t test). Data shown are representative of three independent experiments with similar results.

(G and H) Application of 2 μM Thapsigargin (Tg) in bath solution induced inward currents at −80 mV in control and LPS (100 ng/mL)-treated M2 cells. Respective IV curves of currents and quantitation (5–8 recordings) of current intensity at −80 mV are shown in (G). Bar graphs depict average ± SEM, *p ≤ 0.05 (Student's t test). Data shown are representative of three independent experiments with similar results.

(I) Heatmap showing Log2 Fold changes (N = 3) in selected M1-inflammatory and M2-anti-inflammatory genes in bone marrow-derived macrophages from WT mice treated with IFNγ at 20 ng/mL over medium alone (NS), and corresponding cells from TRPC1$^{-/-}$ mice cultured in presence of IFNγ are shown in columns 1 and 2, respectively.

(J) A 2D scatter plot showing comparison as in (I). The x axis shows Log2 fold change values of IFNγ-treated WT macrophages over unstimulated samples. The y axis shows Log2 fold change values of IFNγ-treated TRPC1$^{-/-}$ over unstimulated TRPC1$^{-/-}$ samples. The color of dots represents statistical significance in differential gene expression. Genes with an adjusted p value < 0.05 were considered as differentially expressed. Red dots denote differentially expressed genes on both comparisons, whereas green dots represent genes that are significant in IFNγ versus NS. Genes differentially expressed in TRPC1$^{-/-}$ (NS versus treated) are shown as purple dots and those non-significant in both conditions are represented by blue dots.

(K) Box plots showing Log2 fold change of the expression of pro- and anti-inflammatory genes in IFNγ treated over unstimulated WT and TRPC1$^{-/-}$ macrophages are shown in boxes 1 and 2, respectively from three independent experiments.

(L) Flow cytometry was performed to measure the difference between wild type and TRPC1$^{-/-}$ of classic internal M1 markers (iNOS$^+$) and M2 markers (Arg1$^+$) and surface M1 (CD80$^+$) and M2 (CD206$^+$) markers. Data shown are representative of three independent experiments with similar results.

Figure 4. *Continued*

(M) Macrophage (M0, M1, and M2) cells from TRPC1$^{-/-}$mice cultured in 6-well plates (2 × 10^6 cells/well) and treated with or without LPS (100 ng/mL) for 6 h. The concentration of pro-inflammatory (IL-6 and IFNγ) cytokines released in the media was performed by ELISA. Data shown are representative of three independent experiments with similar results. Bar graphs depict average ± SD for relative values, NS, non-significant (Student's t test).

(N) Immunoblotting analysis showing the level of expression of wild-type mice versus TRPC1$^{-/-}$ M0, M1, and M2 BMDM polarization pathway genes pNF-κB, NF-κB, pJNK, JNK, pSTAT6, STAT6, pSTAT1, and STAT1 and β-actin. Data shown are representative of three independent experiments with similar results.

as the migration of pSTAT6 into the nucleus was decreased at higher Ca^{2+} concentrations (Figures 3M–3O). These results complement our Ca^{2+} data where higher Ca^{2+} entry was observed in M1 cells when compared with M2 cells (Figure 2I). To understand the importance of the STAT proteins for macrophage transition, we used fludarabine (Flu [5 μM for 24 h], a known STAT1 inhibitor) on M1 cells, which significantly decreased the development of the M1 phenotype (Figures S3D and S3E). In addition, STAT1 inhibitor further decreased the release of IFNγ along with a decrease in iNOS levels (Figures S3F). On the similar lines, M2 activated cells demonstrated a significantly diminished M2 phenotype by the treatment of AS1517499 (AS), a known STAT6 inhibitor (Figures S3G and S3H). These results were further strengthened by reduced expression of Arginase1 and release of IL-10 (an anti-inflammatory cytokine) upon treatment with AS1517499 (Figures S3I). Moreover, a decrease in TRPC1 expression was observed upon the addition of STAT1 inhibitor and a decrease in Orai1 was observed by the addition of STAT6 inhibitor (Figures S3J).

TRPC1$^{-/-}$ mice prevents the M1 phenotype but did not influence the M2 phenotype

Following our findings, we focused on the effects of TRPC1 on the development of the M1 phenotype using TRPC1-deficient mice. M1 macrophages from TRPC1$^{-/-}$ mice treated with IFNγ or LPS displayed no increase in Ca^{2+} influx when compared with the M1 cells obtained from WT mice and treated with IFNγ or LPS (Figures 4A and 4B). Moreover, electrophysiological recordings showed that IFNγ-activated M1 cells from the TRPC1$^{-/-}$ mice displayed no significant increase in the non-selective Ca^{2+} current compared with M1 cells obtained from WT mice (Figures 4C, 4D, and S4A–S4D). Next, IL-4-activated M2 cells obtained from TRPC1$^{-/-}$ were evaluated for Ca^{2+} signaling both in the absence and presence of LPS. M2 cells obtained from TRPC1$^{-/-}$ mice displayed a significantly higher Ca^{2+} influx when compared with M2 cells obtained from WT mice (Figures 4E, 4F, S4G, and S4H). M2 cells from TRPC1$^{-/-}$ mice failed to show a significant increase upon LPS treatment (Figures 4E, 4F, S4E, and s4F). Similarly, activated M2 cells from TRPC1$^{-/-}$ mice displayed high amount of residual current (inwardly rectifying that is observed with Orai1) in comparison with the basal current detected in naive Mφ obtained from WT mice (Figures 4G and 4H). These data further suggest that Mφ and M2 macrophages are mainly activated through the Orai1-dependent Ca^{2+} entry, whereas activated M1 macrophages require TRPC1 channels for Ca^{2+} influx. In line with this, genome-wide analysis also showed that cells obtained from TRPC1$^{-/-}$ mice had a significant decrease in a majority of M1-associated genes, along with a significant increase in most M2-associated genes (Figure 4I). Furthermore, comparison of gene sets that were differentially expressed in TRPC1$^{-/-}$ cells revealed that a set of genes (Nos2, STAT1, CD-86, IL18, CD36, H2-B1, CD68, and others) involved in M1 phenotype responded with decreased expression, whereas increase in genes associated with the M2 phenotype (Arg1, IL1R1, CD209, CD206, TGFβ1, CCl22, CCl17) was observed in the absence of TRPC1 (Figures 4I–4K).

To confirm the role of TRPC1 in macrophage polarization, flow cytometry was performed on Mφ cells obtained from WT or TRPC1$^{-/-}$ mice and internal markers for M1 (iNOS) and M2 (Arginase-1) or surface markers for M1 (CD80) and M2 (CD206) phenotypes were evaluated. We observed a significant decrease in M1 markers upon IFNγ stimulation in TRPC1$^{-/-}$ mice, when compared with wild-type M1 cells (Figure 4L). No change in CD206 and Arginase 1 expression was observed in M2 cells from TRPC1$^{-/-}$ mice, suggesting that the M2 phenotype is intact in TRPC1$^{-/-}$ mice (Figure 4L). ELISA analysis of supernatants from M1 and M2 cells indicated a significant elevation in anti-inflammatory cytokines (e.g., IL-10 and IL-1RII) along with a decrease in pro-inflammatory cytokines derived from TRPC1$^{-/-}$ mice, as compared with their WT counterparts (Figures 4M and S4I). Interesting, LPS stimulation did not decrease the cytokines associated with M2 phenotypes, nor an increase in pro-inflammatory cytokines (such as IL-6, IL-1β, TNFα, and IFNγ) was observed in cells obtained from TRPC1$^{-/-}$ mice (Figures 4M and S4I). Cell lysate from TRPC1$^{-/-}$ cells also displayed a decrease in pNF-κB and pSTAT1, when compared with M1 cells from WT mice (Figures 4N and S4J). In contrast, cells from IL-4 activated M2 mice displayed normal levels of STAT6 phosphorylation when compared with the cells from WT mice (Figure 4N). Together, these results confirm that lack of TRPC1 gene expression proficiently prevents M1 functional phenotype development, whereas the M2 phenotype is not affected and perhaps is dependent on Orai1.

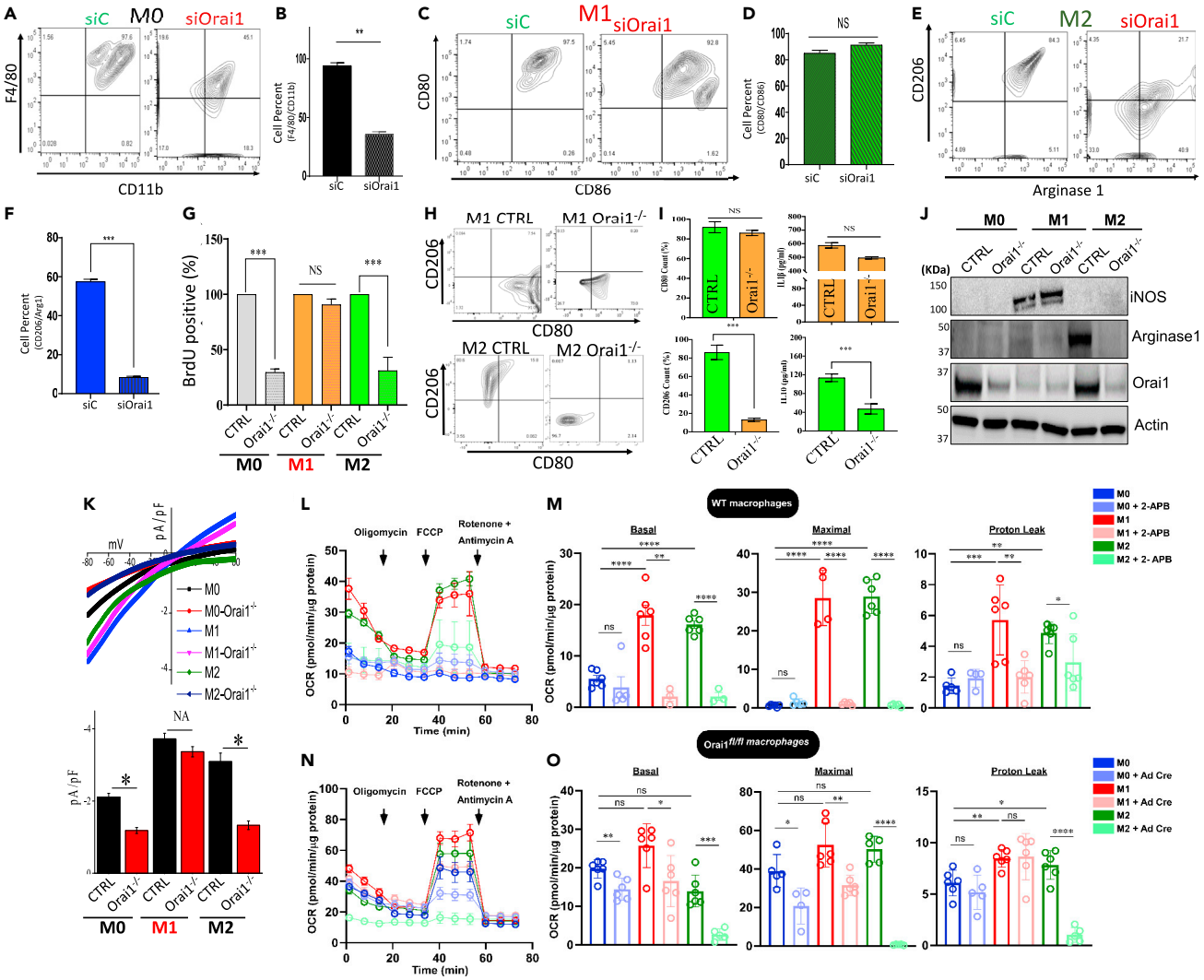

Figure 5. Lack of Orai1 results in impaired M2 phenotype development even with IL4 stimulus

(A) Flow cytometric analysis of macrophage polarization in control siRNA (siC) and siOrai1-treated cells. BMDM cells were harvested 24 h after gene silencing and flow cytometry was performed to measure the levels of F4/80$^+$ and CD11b$^+$. Data shown are representative of three independent experiments with similar results.

(B) Percentage of positive cells for F4/80$^+$ and CD11b$^+$ under the conditions in (A). Data shown are representative of three independent experiments with similar results. Bar graphs depict average ± SD for relative values, **p ≤ 0.001 (Student's t test).

(C) Flow cytometric analysis (CD80$^+$ and CD86$^+$) on macrophage upon respective siRNA treatment. Data shown are representative of three independent experiments.

(D) Percentage of CD80+ and CD86+ positive cells. Bar graphs depict average ± SD for relative values; NS, non-significant (Student's t test) from two independent experiments.

(E) Flow cytometric analysis of CD206$^+$ and Arginase 1$^+$ upon Orai1 silencing. Data shown are representative of three independent experiments with similar results.

(F) Percentage of positive cells for M2 markers of (CD206$^+$ and Arginase1$^+$). Data shown are representative of three independent experiments. Bar graphs depict average ± SD for relative values, ***p ≤ 0.001, NS, non-significant (Student's t test).

(G) Cell proliferation assay for Orai$^{fl/fl}$ with (for Orai1$^{-/-}$) and without (CTRL) Ad.Cre virus. Data shown are representative of three independent experiments. Bar graphs depict BrdU-positive cells ±SD for positive cells, ***p ≤ 0.001 (Student's t test), NS, non-significant. n = 3–4 independent replicates.

(H) Flow cytometer analysis to measure the difference between Orai1$^{fl/fl}$ with and without Ad.Cre virus for M1, M2 markers. Data shown are representative of three independent experiments.

(I) Percentage of positive cells for CD80 and CD206 under the conditions in (H). Data shown are representative of three independent experiments with similar results. Bar graphs depict average ± SD for relative values, NS, non-significant, ***p ≤ 0.001 (Student's t test).

(J) Immunoblot analysis showing the level of expression of iNOS, Arginase1, Orai1, and β-actin of control and Orai1$^{fl/fl}$ mice with and without Ad.Cre virus. Data shown are representative of three independent experiments with similar results.

Figure 5. *Continued*

(K) IV curves of Tg-induced currents at -80 mV in Orai1$^{fl/fl}$ with and without Ad.Cre virus in various cells. Bar graphs represent quantitation (6–8 recordings for each condition) of current intensity at −80 mV. *p ≤ 0.05 (Student's t test).

(L and M) Oxygen consumption rate (OCR) was analyzed in macrophages isolated from WT with and without 2APB (50 μM for 6 h).

(N and O) OCR from WT and Orai1$^{fl/fl}$ macrophages treated with Ad5a iCre for 72 h for M0, M1, and M2 phenotypes. N = 3 performed in duplicate. Basal, maximal respiration, and proton leak analysis of macrophages isolated from WT with and without 2APB (50 μM for 6 h) WT and Orai1$^{fl/fl}$ macrophages treated with Ad5a iCre for 72 h. Mean ± SEM, n = 3, *p < 0.05, **p < 0.01, ***p < 0.001, ****p < 0.0001. n.s., not significant.

Loss of Orai1 expression results in loss of M2 phenotype development even with IL-4 stimulus

We next evaluated the physiological effect of Orai1 channels on Mφ cell transition. Naive Mφ, M1, and M2 cells were transfected with non-targeting siRNA (SiC, for control) or Orai1siRNA (siOrai1), and activation of M1 or M2 phenotype was evaluated. Although silencing of Orai1 in naive Mφ cells displayed expression of the classical F4/80^{+}CD11b^{+} markers, the number of positive cells was decreased when compared with control siRNA-treated cells (Figures 5A and 5B). In contrast, activated M1 cells were not significantly affected by the transfection of siOrai1 and were able to maintain the same levels of M1 surface markers (CD80 + CD86) (Figures 5C and 5D). Nevertheless, activated M2 cells transfected with siOrai1 had considerably low levels of M2 phenotype markers (Figures 5E and 5F). To establish the role of Orai1 in macrophage function, we obtained Mφ cells from Orai$^{fl/fl}$ mice and treated them with Ad.Cre virus to knock down Orai1 expression specifically in Mφ cells (Figure S5A). Loss of Orai1 significantly reduced cell viability in naive Mφ and M2 cells, without affecting the M1 cells (Figure 5G). Flow cytometry further showed no significant difference in the M1 surface markers; however, a significant decrease in the level of M2 markers was observed in Orai$^{-/-}$ mice cells (Figures 5H and 5I). However, again a decrease in cell numbers was observed, suggesting that naive Mφ are affected by the lack of Orai1 (Figures 5H and 5I). ELISA analysis of supernatants from M2 cells from Orai1$^{-/-}$ mice (Orai1$^{fl/fl}$ + Ad.Cre virus) displayed a significant decrease in anti-inflammatory cytokine IL-10, as compared with control cells (no Ad.Cre virus) (Figure 5I). Lack of Orai1 did not affect cytokines associated with the M1 phenotype (Figure 5I). Immunoblot analysis further showed no change in iNOS expression once the Orai1 gene was inactivated (Figures 5J and S5B). In contrast, a significant decrease in Arginase1 expression was observed in M2 activated cells of Orai1$^{-/-}$ (Figure 5J).

Functional characterization of the channel activity also showed that loss of Orai1 only affected Ca^{2+} currents in the naive and M2 phenotypes, whereas the M1 phenotype showed similar current levels as observed in wild-type cells (Figure 5K). Agonist-induced Ca^{2+} release followed by calcium entry are shown to be essential for mitochondrial Ca^{2+} uptake that modulates ATP synthesis and (Daw et al., 2020; Hawkins et al., 2010). Similarly, metabolism has been suggested as a key regulator for macrophage differentiation; however, it remains unclear whether Orai-mediated Ca^{2+} entry modulates mitochondrial bioenergetics. Thus, to evaluate the mitochondrial bioenergetics, we measured the oxygen consumption rate (OCR) as a readout for the analysis of mitochondrial function in naive M1 and M2 cells (Nemani et al., 2020). Interesting, naive Mφ exhibited low basal and maximal OCR, which was increased in macrophages treated with IFNγ (20 ng/mL for M1) or IL-4 (20 ng/mL for M2) (Figures 5L and 5M). Moreover, inhibition of Ca^{2+} entry by the addition of 2-APB (50 μM) significantly suppressed the basal and maximal OCR in M1 and M2 macrophages, suggesting that loss of Ca^{2+} entry inhibits mitochondrial function (Figures 5L and 5M). Since 2APB effect is nonselective, we next tested whether genetic ablation of Orai1 in macrophages also alters mitochondrial OCR. Orai1$^{fl/fl}$ macrophages were infected with Ad.Cre virus for 48 h followed by IFNγ or IL-4 stimulation for 24 h to develop the pro-inflammatory (M1) and anti-inflammatory (M2) phenotypes. The M1 and M2 macrophages exhibited higher basal and maximal respiration states compared with the naïve Mφ (Figures 5N and 5O). However, loss of Orai1 showed remarkably lower levels of mitochondrial OCR (basal and maximal) especially in the M2 phenotype (Figure 5O). Collectively, these data indicate that loss of Orai1 prevents mitochondrial bioenergetics that specifically modulates M2 polarization.

Deletion of Orai1 promotes macrophage mitochondrial shape transition in M2 cells

Having observed remarkable changes in mitochondrial OCR, we next assessed whether mitochondrial morphology, including its length, perimeter, and area, is also altered in these conditions (Daw et al., 2020; Nemani et al., 2018). Individual cells were loaded with mitochondrial membrane potential ($\Delta\Psi_m$) indicator DHR123 and a cationic dye TMRE to monitor changes in mitochondrial morphology and $\Delta\Psi_m$. Analysis of $\Delta\Psi_m$ and mitochondrial length revealed that the polarized M1 and M2 macrophages from control mice (-Ad cre) exhibited characteristically distinct phenotypic variations in mitochondrial length, area, and

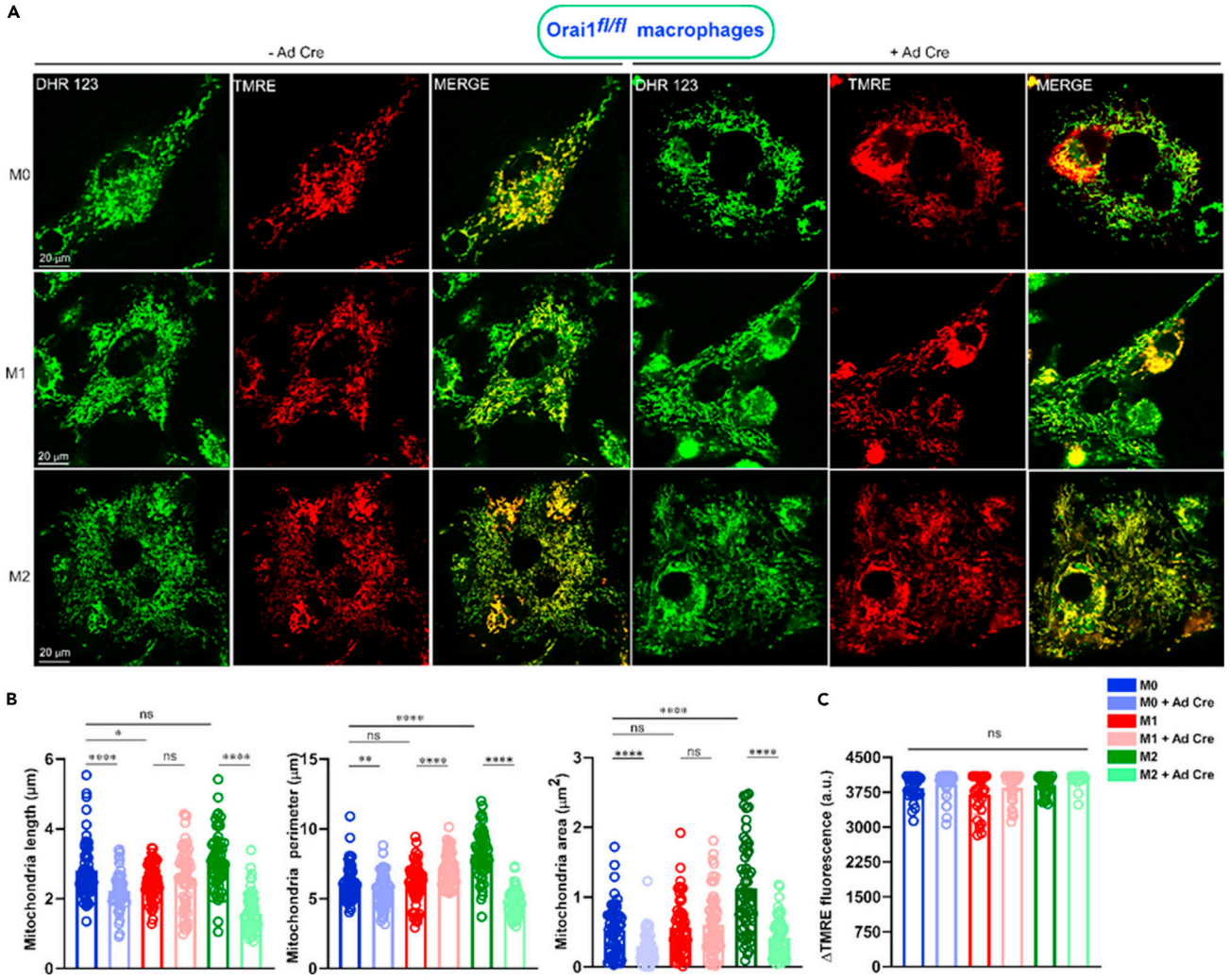

Figure 6. Orai1 deletion exhibits macrophage mitochondrial shape transition

(A and B) Representative confocal micrographs (60×) showing mitochondrial phenotype assessed in macrophages derived from Orai1$^{fl/fl}$ mice with and without Ad.Cre virus treatment for 72 h. Macrophages were stained with DHR123 and TMRE for 30 min and confocal images were acquired immediately. Scale bar, 20 μm. Images shown are representative of three independent experiments. (B) Quantification (mean ± SEM) of mitochondrial length, perimeter, and mitochondrial area are shown as bar graph in (B). *p < 0.05, **p < 0.01, ****p < 0.0001. n.s., not significant.

(C) Measurement of mitochondrial membrane potential as TMRE fluorescence retention in the mitochondria. Mean ± SEM, n = 3, n.s., not significant.

perimeter (Figures 6A and 6B). In comparison with control macrophages, naive and M2, but not M1, macrophages infected with the Ad.Cre virus showed a marked reduction in mitochondrial length and area (Figures 6A and 6B). The significant decrease in the mitochondrial perimeter, length, and area, but not $\Delta\Psi m$, in naive Mφ and M2 cells obtained from Orai1$^{-/-}$ mice suggests that the mitochondrial shape transition events could be the main reason that linearly affected mitochondrial OCR and bioenergetics. The results strongly suggest Orai1-mediated Ca^{2+} entry is crucial for mitochondrial bioenergetics in naive Mφ and in the activation of the M2 phenotype.

Alterations in SOCE channel expression dictates M1/M2 transformation

The results presented thus far suggest that Orai1 is essential for the M2 phenotype but did not affect the M1 phenotype, which was dependent on TRPC1 function. Thus, next, we evaluated if alterations in the expression of these Ca^{2+} entry channels (Orai1 and TRPC1) could modulate the M1 and M2 transition and establish its role in macrophage plasticity. To achieve our objective, we transfected with respective siRNA and at the same time overexpressed the alternate Ca^{2+} entry channel and compared the production

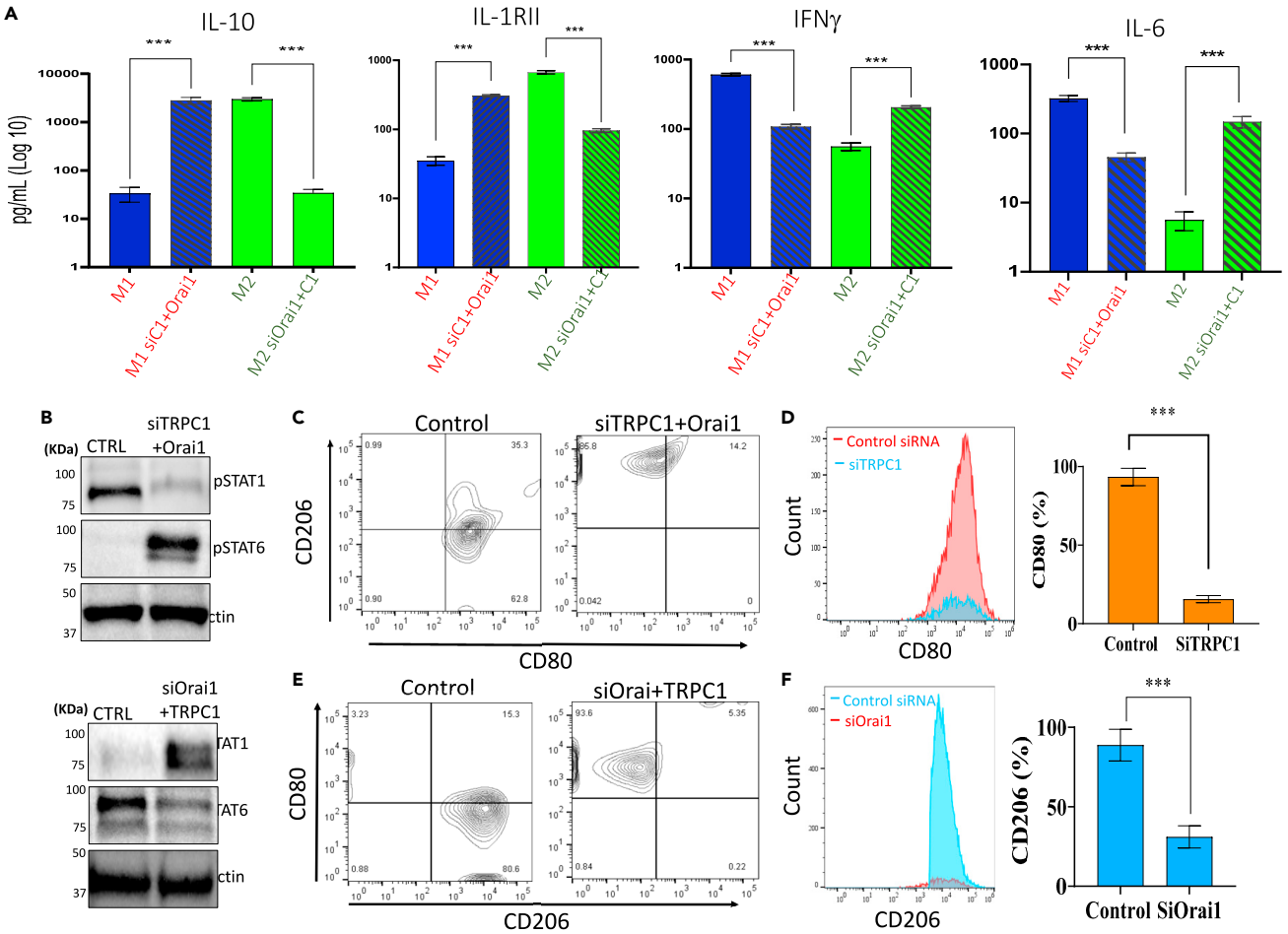

Figure 7. Ca^{2+} influx via TRPC1 channels mediate M1 phenotype polarization, and M2 polarization is dependent on Orai1 channels

(A) Cytokine released in M1 (+IFNγ for 24 h) cells along with silencing of TRPC1 and overexpressing Orai1 and in M2 (+IL-4 for 24 h) cells in Orai1 silenced cells, but overexpressing TRPC1 gene was measured by ELISA. Data shown are representative of three independent experiments. Bar graphs depict average ± SD for relative values, ***$p \leq 0.001$ (Student's t test).

(B) Immunoblot analysis showing the level of expression of pSTAT1 and pSTAT6 in conditions as labeled. Data shown are representative of three independent experiments.

(C–F) Flow cytometry analysis of individual groups as labeled were used to measure levels of M1 ($CD80^+$) and M2 markers ($CD206^+$) in various conditions. Data shown are representative of three independent experiments. Percentage of positive cells for M1 ($CD80^+$) and M2 ($CD206^+$) under the conditions are shown as bar graph depicting average ± SD for relative values, ***$p \leq 0.001$ (Student's t test). Data shown are representative of three independent experiments.

of pro-inflammatory M1 and anti-inflammatory M2 cytokines. IFNγ-activated M1 cells were transfected with siRNA that targets TRPC1 (siTRPC1), along with overexpressing Orai1. IL-6 and IFNγ (which indicate the M1 phenotype) levels were significantly lower in supernatants of M1 activated cells that overexpress Orai1 but were silenced for TRPC1 (Figure 7A). In contrast, levels of cytokines that are classical for M2 activation (IL-10 and IL1RII) were increased in cells that overexpressed Orai1 and were silenced for TRPC1 (Figure 7A). Similarly, IL-4-activated M2 cells were transfected with Orai1siRNA along with TRPC1 overexpression, which displayed high levels of M1-related cytokines and low levels of M2 cytokines (Figure 7A). Consistent with these results, immunoblot analysis showed a significant decrease in the phosphorylation of pSTAT1 in TRPC1-silenced but Orai1-overexpressed cells (Figures 7B and S5C). In contrast, a significant increase in the phosphorylation of STAT6 was observed in TRPC1-silenced but Orai1-overexpressed cells (Figures 7B and S5C). Similarly, decrease in Orai1 along with an increase in TRPC1 expression increased pSTAT1 phosphorylation, along with a decrease in pSTAT6 phosphorylation (Figures 7B and S5C). Of interest, flow cytometry analysis also showed that M1 activated cells that were transfected with siTRPC1 and overexpressed Orai1 displayed reduced surface M1 marker (CD80), in conjunction with an increase in M2

marker (Figures 7C and 7D). Correspondingly, M2 activated cells transfected with siOrai1 along with TRPC1 overexpression also displayed significantly lower levels of the M2 marker (CD206) while showing high levels of the M1 marker (CD80) (Figures 7E and 7F). Together, these results demonstrate that TRPC1 channels play a key role in the development of the IFNγ-induced M1 functional phenotype, whereas Orai1 is critical for the IL4-induced M2 phenotype. Moreover, alterations in their expression dictate the M1 to M2 or M2 to M1 transformation, which establish a clear separation of essential Ca^{2+} influx channels and identify mechanisms that could lead to macrophages transformation by altering the expression of the SOCE channels.

DISCUSSION

Macrophages promote the induction of infectious inflammation followed by resolution to maintain the innate immune surveillance (Feske et al., 2015; Italiani and Boraschi, 2015; Werz et al., 2018). Macrophages display two distinct phenotypes: classically activated M1 and alternatively activated M2 macrophages that are regulated by the environment (Cerny and Striz, 2019), but the mechanism of its plasticity is not clear. Our study shows that Ca^{2+} influx is essential for macrophage polarization. We identified a specific function of TRPC1/Orai1 in the activation of M1/M2 phenotypes, respectively. Lymphocytes need Ca^{2+} channel activity for their function (Demaurex and Nunes, 2016). However, our results showed that not only macrophage activation and mitochondrial bioenergetics but also its polarization is Ca^{2+} dependent. Ca^{2+} entry channel blockers decreased macrophage polarization and its proliferation/viability. Of interest, in the absence of TRPC1/Orai1 expression a decrease in cell proliferation, even upon LPS stimulation, which is a known TLR activator, suggests that Ca^{2+} influx is indispensable for appropriate macrophage function. Furthermore, Ca^{2+} signaling through distinct Ca^{2+} entry channels plays a key role in macrophage functions, including the release of pro- and anti-inflammatory cytokines, phagocytosis, and apoptosis. Our data using Orai1 null macrophages showed that Orai1 channels are essential for macrophage proliferation at the naive and activated M2 modes along with a decrease in OCR and mitochondrial morphology, whereas TRPC1 specifically modulated the M1 phenotypes, suggesting that distinct Ca^{2+} entry channels are involved in various polarized states of macrophage.

Identifying mechanisms that drive macrophage heterogeneity is critical for the development of therapeutic strategies. The aptitude to shift macrophage profiles in response to changes in the microenvironment is crucial for initiation/resolution of inflammation, as well as tissue repair (Gandhirajan et al., 2013; Jha et al., 2015; Kim et al., 2017; Porcheray et al., 2005). Of importance, an increase in TRPC1 expression was observed upon LPS treatment, in both naive and M2 macrophages. Furthermore, activated M2 cells showed an increase of M1 markers, along with a decrease in M2 markers, when treated with LPS. Ca^{2+} levels also dictated the specificity that modulates the M1 and M2 phenotypes, respectively, as increasing extracellular Ca^{2+} promoted STAT1 phosphorylation but decreased pSTAT6 expression and its migration into the nucleus. These results show that macrophage phenotype is heterogeneous and multiple polarization states are achieved with certain stimulations that regulate gene expression and the epigenome (Ivashkiv, 2013). The presence of external stimulus is responsible for the direction of the differentiation of immune cells, and the stimulus could be directed toward lineages specificity to control the infecting pathogen or induce tissue repair (Blagih and Jones, 2012). Our data show that IFNγ treatment increases TRPC1 expression, whereas IL-4 was required to increase Orai1 expression, and alterations in their expression can induce M1 or M2 phenotypes. To identify downstream signaling events associated with these phenotypic changes we studied IRF/STAT/NF-κB signaling, a key pathway in controlling macrophage polarization. Toll-like receptor signaling (mainly TLR4) drives the M1 phenotype through the myeloid differentiation factor 88 (MyD88) that results in the activation of nuclear factor kappa B (NF-κB) (Mosser and Edwards, 2008; Orecchioni et al., 2019; Wang et al., 2014). In contrast, studies have shown that IL-4-polarized M2 macrophage phenotypes are activated by the STAT6 signaling pathway, through the IL-4 receptor alpha (IL-4Ra) (Bouhlel et al., 2007; Chawla, 2010; Mantovani et al., 2002). These results are consistent with our studies where TRPC1 activated the NF-κB/STAT1 pathway, whereas Orai1 was essential for the STAT6 pathway. pNF-κB and pSTAT1 functionally bind to the TRPC1 promoter to increase its expression, which was essential for the development of the M1 phenotype.

Elucidating the activated states of macrophages and targeting the polarization process, along with the transition from M1 to M2 or vice versa, might serve as a diagnostic or therapeutic strategy for multiple diseases. Significantly, our data show that Mφ polarization can be rapidly induced and reversed or be re-polarized by complex and interacting endogenous cellular signaling pathways and their modulators. Although multiple pathways and several important modulators have been described as essential for subset

differentiation (Van den Bossche et al., 2016), our data also identify that the expression of Ca^{2+} entry channels is a vital part of these modulators. Macrophage cells show distinct Ca^{2+} influx channels, and our results highlight the critical function of the TRPC1-dependent Ca^{2+} influx in mediating the M1 and Orai1-dependent Ca^{2+} influx mediating the M2 functional phenotypes. Furthermore, in the absence of functional TRPC1 or Orai1 channels, we demonstrate an inability of macrophages to maintain the polarization stage. In addition, impairment of TRPC1 channels obstructed M1 function and a decline in phagocytosis activity in M1 phenotype cells was observed. It is accepted that phagocytosis is the most important event in the immune response, and macrophage activation signifies an up-regulation of the innate immune response (Davidson and Wood, 2020; Gray et al., 2016; Vaeth et al., 2015). Although loss of STIM1 did not blunt macrophage function, nonselective inhibition of Ca^{2+} signaling did impair phagocytosis and priming of T cells (Vaeth et al., 2015). Correspondingly, loss of SOCE leads to M2-activated decline in angiogenesis activity, as well as decrease in mitochondrial bioenergetics is observed in Orai1$^{-/-}$ cells. A decrease in vascular endothelial growth factor (VEGF) was also observed when the cells lack SOCE channel activation. Knockdown of VEGF has been shown to block macrophage recruitment into tumor tissues, causing major disruptions in the tissue healing process (Grivennikov et al., 2010), which provides a new function for these channels. Previous studies had shown that Ca^{2+} entry through Orai1 led to the insertion of vesicles containing TRPC1 (Cheng et al., 2011); however, Orai1$^{-/-}$ M1 cells showed normal TRPC1-like currents, suggesting that perhaps other Orai2/3 channels could also be critical for TRPC1 function and more research is needed to fully establish their role in the M1 phenotype.

Our findings not only answered the question on the importance of Ca^{2+} influx in macrophage polarization but also identified the Ca^{2+} channel involved in this process. Loss of Orai1 has a damaging impact on the activation of naive macrophages and weakens M2 activation essential for immune resolution. We also established the effects on cytokine release when either TRPC1 or Orai1 is downregulated. TRPC1 downregulation, along with Orai1 overexpression in M1 activated macrophages showed a decrease in markers depicting the M1 phenotype along with an increase in M2 markers. Similarly, silencing Orai1 and overexpressing TRPC1 in M2 activated macrophages showed the opposite results, suggesting that macrophage polarization is based on specific Ca^{2+} channel expression. Not only surface markers but also cytokines were altered upon changes in Ca^{2+} entry channel expression, thereby directly attesting the phenotypic transformation between M1 and M2 cells is strictly dependent on the expression of these distinct channels. Ca^{2+} entry channels are an intricate phenomenon in the physiology and pathophysiology of inflammation and immune system (Ahuja et al., 2017; Nascimento Da Conceicao et al., 2019; Parenti et al., 2016; Vaeth et al., 2015), but their role in macrophage polarization is not characterized. These studies support our findings, where we observed that cells from TRPC1$^{-/-}$ mice not only showed decreased Ca^{2+} influx but LPS stimulation also prevented the potentiation of Ca^{2+} influx. The absence of the TRPC1 channel is responsible for the complete lack of M1 macrophage polarization, even at the pathway level, as we show no STAT1 or NF-κB activation. On the contrary, M2 polarization seems to develop with no problem, and both surface (CD206) and internal markers (Arginase 1) along with anti-inflammatory cytokines release were at normal levels, whereas loss of Orai1 specifically altered the M2 phenotype. In conclusion, macrophage activation and its polarization depend on calcium channels that are coordinated by either TRPC1 or Orai1. Moreover, deficiency of the TRPC1 channel impairs M1 phenotype development, whereas loss of Orai1 prevents the M2 phenotype by inhibiting mitochondrial function as M2 are dependent on energetics from the tricarboxylic acid cycle (Gray et al., 2016). These results demonstrate the importance of these regulatory mechanisms that modulate gene expression, and together, these data may become a landmark in providing basic knowledge for therapeutic strategies for initiation of inflammation and to induce tissue repair.

Limitations of the study

This study demonstrates the regulatory mechanisms that modulate macrophage polarization. Although using primary macrophages we are able to show that TRPC1 and Orai1 distinctly modulate the M1 and M2 phenotypes, experiments using *in vivo* conditions are needed to see that alteration in various calcium channels lead to the M1 and M2 phenotypes. In addition, ER and mitochondrial calcium need to evaluated to see if they also modulate macrophage polarization.

STAR★METHODS

Detailed methods are provided in the online version of this paper and include the following:

- KEY RESOURCES TABLE

SUPPLEMENTAL INFORMATION

Supplemental information can be found online at https://doi.org/10.1016/j.isci.2021.103339.

ACKNOWLEDGMENTS

This work was funded by grant support from the National Institutes of Health (R01DE017102; R01DE022765) awarded to B.B.S. This research was funded by the National Institutes of Health (R01GM109882, R01HL086699, R01HL142673, R01GM135760, and 1S10RR027327) to M.M. This work was partly supported by DOD/DHP-CDMRP PR181598P-1 and San Antonio Partnership for Precision Therapeutics (SAPPT) to M.M. The funders had no further role in study design, data analysis, and/or interpretation of the data. Flow Cytometry Facility is supported by UTHSCSA, NIH-NCI P30 CA054174-20, and UL1 TR001120.

AUTHOR CONTRIBUTIONS

Conceptualization, methodology, and analysis, V.N.D.C., B.B.M., M.M., and B.B.S. Animal genotyping, experiments, data analysis, and interpretation, K.R., M.V., S.M., N.V., and M.M. Experimental investigation, V.N.D.C., Y.S., K.R., A.C., A.R., M.V., B.D., S.M., G.A.K., M.M., and B.B.M. Writing–review and editing, V.N.D.C., N.V., B.B.M., D.L.G., M.M., and B.B.S.

DECLARATION OF INTERESTS

The authors declare no competing interests.

Received: August 11, 2021
Revised: September 30, 2021
Accepted: October 20, 2021
Published: November 19, 2021

REFERENCES

Ahuja, M., Schwartz, D.M., Tandon, M., Son, A., Zeng, M., Swaim, W., Eckhaus, M., Hoffman, V., Cui, Y., Xiao, B., et al. (2017). Orai1-Mediated antimicrobial secretion from pancreatic acini shapes the gut microbiome and regulates gut innate immunity. Cell Metab. *25*, 635–646.

Benoit, M., Desnues, B., and Mege, J.L. (2008). Macrophage polarization in bacterial infections. J. Immunol. *181*, 3733–3739.

Blagih, J., and Jones, R.G. (2012). Polarizing macrophages through reprogramming of glucose metabolism. Cell Metab. *15*, 793–795.

Bollimuntha, S., Selvaraj, S., and Singh, B.B. (2011). Emerging roles of cannonical TRP channels in neuronal function. Adv. Exp. Med. Biol. *704*, 573–593.

Van den Bossche, J., Baardman, J., Otto, N.A., van der Velden, S., Neele, A.E., van den Berg, S.M., Luque-Martin, R., Chen, H.J., Boshuizen, M.C., Ahmed, M., et al. (2016). Mitochondrial dysfunction prevents repolarization of inflammatory macrophages. Cell Rep. *17*, 684–696.

Bouhlel, M.A., Derudas, B., Rigamonti, E., Dievart, R., Brozek, J., Haulon, S., Zawadzki, C.,

Jude, B., Torpier, G., Marx, N., et al. (2007). PPARgamma activation primes human monocytes into alternative M2 macrophages with anti-inflammatory properties. Cell Metab. *6*, 137–143.

Brodsky, I.E. (2020). JAK-ing into M1/M2 polarization SteErs salmonella-containing macrophages away from immune attack to promote bacterial persistence. Cell Host Microbe *27*, 3–5.

Cairo, G., Recalcati, S., Mantovani, A., and Locati, M. (2011). Iron trafficking and metabolism in macrophages: contribution to the polarized phenotype. Trends Immunol. *32*, 241–247.

Cerny, J., and Striz, I. (2019). Adaptive innate immunity or innate adaptive immunity? Clin. Sci. (Lond) *133*, 1549–1565.

Chauhan, A., Sun, Y., Sukumaran, P., Quenum Zangbede, F.O., Jondle, C.N., Sharma, A., Evans, D.L., Chauhan, P., Szlabick, R.E., Aaland, M.O., et al. (2018). M1 macrophage polarization is dependent on TRPC1-mediated calcium entry. iScience *8*, 85–102.

Chawla, A. (2010). Control of macrophage activation and function by PPARs. Circ. Res. *106*, 1559–1569.

Cheng, K.T., Liu, X., Ong, H.L., Sai, W., and Ambudkar, I.S. (2011). Local Ca^{2}+ entry via Orai1 regulates plasma membrane recruitment of TRPC1 and controls cytosolic Ca^{2}+ signals required for specific cell functions. PLoS Biol. *9*, e1001025.

Clapham, D.E. (2007). Calcium signaling. Cell *131*, 1047–1058.

Davidson, A.J., and Wood, W. (2020). Macrophages use distinct actin regulators to switch engulfment strategies and EnsurevPhagocytic plasticity in vivo. Cell Rep. *31*, 107692.

Daw, C.C., Ramachandran, K., Enslow, B.T., Maity, S., Bursic, B., Novello, M.J., Rubannelsonkumar, C.S., Mashal, A.H., Ravichandran, J., Bakewell, T.M., et al. (2020). Lactate elicits ER-mitochondrial Mg(2+) dynamics to integrate cellular metabolism. Cell *183*, 474–489.e17.

Demaurex, N., and Nunes, P. (2016). The role of STIM and ORAI proteins in phagocytic immune cells. Am. J. Physiol. Cell Physiol. *310*, C496–C508.

Feske, S., Gwack, Y., Prakriya, M., Srikanth, S., Puppel, S.H., Tanasa, B., Hogan, P.G., Lewis, R.S., Daly, M., and Rao, A. (2006). A mutation in Orai1 causes immune deficiency by abrogating CRAC channel function. Nature *441*, 179–185.

Feske, S., Wulff, H., and Skolnik, E.Y. (2015). Ion channels in innate and adaptive immunity. Annu. Rev. Immunol. *33*, 291–353.

Gandhirajan, R.K., Meng, S., Chandramoorthy, H.C., Mallilankaraman, K., Mancarella, S., Gao, H., Razmpour, R., Yang, X.F., Houser, S.R., Chen, J., et al. (2013). Blockade of NOX2 and STIM1 signaling limits lipopolysaccharide-induced vascular inflammation. J. Clin. Invest. *123*, 887–902.

Gautier, E.L., Shay, T., Miller, J., Greter, M., Jakubzick, C., Ivanov, S., Helft, J., Chow, A., Elpek, K.G., Gordonov, S., et al. (2012). Gene-expression profiles and transcriptional regulatory pathways that underlie the identity and diversity of mouse tissue macrophages. Nat. Immunol. *13*, 1118–1128.

Gray, M.A., Choy, C.H., Dayam, R.M., Ospina-Escobar, E., Somerville, A., Xiao, X., Ferguson, S.M., and Botelho, R.J. (2016). Phagocytosis enhances lysosomal and bactericidal properties by activating the transcription factor TFEB. Curr. Biol. *26*, 1955–1964.

Grivennikov, S.I., Greten, F.R., and Karin, M. (2010). Immunity, inflammation, and cancer. Cell *140*, 883–899.

Han, Y.H., Kim, H.J., Na, H., Nam, M.W., Kim, J.Y., Kim, J.S., Koo, S.H., and Lee, M.O. (2017). RORalpha induces KLF4-mediated M2 polarization in the liver macrophages that protect against Nonalcoholic steatohepatitis. Cell Rep. *20*, 124–135.

Hawkins, B.J., Irrinki, K.M., Mallilankaraman, K., Lien, Y.C., Wang, Y., Bhanumathy, C.D., Subbiah, R., Ritchie, M.F., Soboloff, J., Baba, Y., et al. (2010). S-glutathionylation activates STIM1 and alters mitochondrial homeostasis. J. Cell Biol. *190*, 391–405.

Italiani, P., and Boraschi, D. (2015). New insights into tissue macrophages: from their Origin to the development of memory. Immune Netw. *15*, 167–176.

Ivashkiv, L.B. (2013). Epigenetic regulation of macrophage polarization and function. Trends Immunol. *34*, 216–223.

Izquierdo-Torres, E., Hernandez-Oliveras, A., Fuentes-Garcia, G., and Zarain-Herzberg, A. (2020). Calcium signaling and epigenetics: a key point to understand carcinogenesis. Cell Calcium *91*, 102285.

Jha, A.K., Huang, S.C., Sergushichev, A., Lampropoulou, V., Ivanova, Y., Loginicheva, E., Chmielewski, K., Stewart, K.M., Ashall, J., Everts, B., et al. (2015). Network integration of parallel metabolic and transcriptional data reveals metabolic modules that regulate macrophage polarization. Immunity *42*, 419–430.

Kar, P., and Parekh, A.B. (2015). Distinct spatial Ca2+ signatures selectively activate different NFAT transcription factor isoforms. Mol. Cell *58*, 232–243.

Kim, D., Lee, H., Koh, J., Ko, J.S., Yoon, B.R., Jeon, Y.K., Cho, Y.M., Kim, T.H., Suh, Y.S., Lee, H.J., et al. (2017). Cytosolic pellino-1-mediated K63-linked ubiquitination of IRF5 in M1 macrophages regulates glucose intolerance in obesity. Cell Rep. *20*, 832–845.

Li, H., Rao, A., and Hogan, P.G. (2011). Interaction of calcineurin with substrates and targeting proteins. Trends Cell Biol. *21*, 91–103.

Liao, Y., Erxleben, C., Abramowitz, J., Flockerzi, V., Zhu, M.X., Armstrong, D.L., and Birnbaumer, L. (2008). Functional interactions among Orai1, TRPCs, and STIM1 suggest a STIM-regulated heteromeric Orai/TRPC model for SOCE/Icrac channels. Proc. Natl. Acad. Sci. U S A *105*, 2895–2900.

Lin, Y.,P., Bakowski, D., Mirams, G.R., and Parekh, A.B. (2019). Selective recruitment of different Ca $^{2+}$-dependent transcription factors by STIM1-Orai1 channel clusters. Nat. Commun. *10*, 2516–2528.

Liu, Y.Z., Wang, Y.X., and Jiang, C.L. (2017). Inflammation: the common pathway of stress-related diseases. Front Hum. Neurosci. *11*, 316.

Mantovani, A., Sozzani, S., Locati, M., Allavena, P., and Sica, A. (2002). Macrophage polarization: tumor-associated macrophages as a paradigm for polarized M2 mononuclear phagocytes. Trends Immunol. *23*, 549–555.

Mosser, D.M., and Edwards, J.P. (2008). Exploring the full spectrum of macrophage activation. Nat. Rev. Immunol. *8*, 958–969.

Murray, P.J., Allen, J.E., Biswas, S.K., Fisher, E.A., Gilroy, D.W., Goerdt, S., Gordon, S., Hamilton, J.A., Ivashkiv, L.B., Lawrence, T., et al. (2014). Macrophage activation and polarization: nomenclature and experimental guidelines. Immunity *41*, 14–20.

Nascimento Da Conceicao, V., Sun, Y., Zboril, E.K., De la Chapa, J.J., and Singh, B.B. (2019). Loss of Ca(2+) entry via Orai-TRPC1 induces ER stress, initiating immune activation in macrophages. J. Cell Sci. *133*, jcs237610.

Nemani, N., Carvalho, E., Tomar, D., Dong, Z., Ketschek, A., Breves, S.L., Jana, F., Worth, A.M., Heffler, J., Palaniappan, P., et al. (2018). MIRO-1 determines mitochondrial shape transition upon GPCR activation and Ca(2+) stress. Cell Rep. *23*, 1005–1019.

Nemani, N., Dong, Z., Daw, C.C., Madaris, T.R., Ramachandran, K., Enslow, B.T., Rubannelsonkumar, C.S., Shanmughapriya, S., Mallireddigari, V., Maity, S., et al. (2020). Mitochondrial pyruvate and fatty acid flux modulate MICU1-dependent control of MCU activity. Sci. Signal. *13*, eaaz6206.

Ong, H.L., de Souza, L.B., and Ambudkar, I.S. (2016). Role of TRPC channels in store-operated calcium entry. Adv. Exp. Med. Biol. *898*, 87–109.

Orecchioni, M., Ghosheh, Y., Pramod, A.B., and Ley, K. (2019). Macrophage polarization: different gene signatures in M1(LPS+) vs. classically and M2(LPS-) vs. alternatively activated macrophages. Front Immunol. *10*, 1084.

Pagiatakis, C., Musolino, E., Gornati, R., Bernardini, G., and Papait, R. (2019). Epigenetics of aging and disease: a brief overview. Aging Clin. Exp. Res. *33*, 737–745.

Parekh, A.B., and Putney, J.W., Jr. (2005). Store-operated calcium channels. Physiol. Rev. *85*, 1757–1810.

Parenti, A., De Logu, F., Geppetti, P., and Benemei, S. (2016). What is the evidence for the role of TRP channels in inflammatory and immune cells? Br. J. Pharmacol. *173*, 953–969.

Porcheray, F., Viaud, S., Rimaniol, A.C., Leone, C., Samah, B., Dereuddre-Bosquet, N., Dormont, D., and Gras, G. (2005). Macrophage activation switching: an asset for the resolution of inflammation. Clin. Exp. Immunol. *142*, 481–489.

Raynal, N.J., Lee, J.T., Wang, Y., Beaudry, A., Madireddi, P., Garriga, J., Malouf, G.G., Dumont, S., Dettman, E.J., Gharibyan, V., et al. (2016). Targeting calcium signaling induces epigenetic reactivation of tumor suppressor genes in cancer. Cancer Res. *76*, 1494–1505.

Selvaraj, S., Sun, Y., Watt, J.A., Wang, S., Lei, S., Birnbaumer, L., and Singh, B.B. (2012). Neurotoxin-induced ER stress in mouse dopaminergic neurons involves downregulation of TRPC1 and inhibition of AKT/mTOR signaling. J. Clin. Invest. *122*, 1354–1367.

Singh, B.B., Liu, X., and Ambudkar, I.S. (2000). Expression of truncated transient receptor potemntial protein 1a (TRPC1a). Eviddnce that the TRpc1 C terminus modulates store-operated Ca2+ entry. J. Biol. Chem. *275*, 36483–36486.

Singh, B.B., Lockwich, T.P., Bandyopadhyay, B.C., Liu, X., Bollimuntha, S., Brazer, S.C., Combs, C., Das, S., Leenders, A.G., Sheng, Z.H., et al. (2004). VAMP2-dependent exocytosis regulates plasma membrane insertion of TRPC3 channels and contributes to agonist-stimulated Ca2+ influx. Mol. Cell *15*, 635–646.

Sukumaran, P., Schaar, A., Sun, Y., and Singh, B.B. (2016). Functional role of TRP channels in modulating ER stress and autophagy. Cell Calcium *60*, 123–132.

Sun, Y., Sukumaran, P., Varma, A., Derry, S., Sahmoun, A.E., and Singh, B.B. (2014). Cholesterol-induced activation of TRPM7 regulates cell proliferation, migration, and viability of human prostate cells. Biochim. Biophys. Acta *1843*, 1839–1850.

Trouplin, V., Boucherit, N., Gorvel, L., Conti, F., Mottola, G., and Ghigo, E. (2013). Bone marrow-derived macrophage production. J. Vis. Exp. *22*, e50966.

Vaeth, M., Zee, I., Concepcion, A.R., Maus, M., Shaw, P., Portal-Celhay, C., Zahra, A., Kozhaya, L., Weidinger, C., Philips, J., et al. (2015). Ca2+ signaling but not store-operated Ca2+ entry is required for the function of macrophages and dendritic cells. J. Immunol. *195*, 1202–1217.

Viola, A., Munari, F., Sanchez-Rodriguez, R., Scolaro, T., and Castegna, A. (2019). The metabolic signature of macrophage responses. Front Immunol. *10*, 1462.

Waldron, R.T., Short, A.D., and Gill, D.L. (1997). Store-operated Ca2+ entry and coupling to Ca2+ pool depletion in thapsigargin-resistant cells. J. Biol. Chem. *272*, 6440–6447.

Wang, N., Liang, H., and Zen, K. (2014). Molecular mechanisms that influence the macrophage m1-m2 polarization balance. Front Immunol. *5*, 614.

Werz, O., Gerstmeier, J., Libreros, S., De la Rosa, X., Werner, M., Norris, P.C., Chiang, N., and Serhan, C.N. (2018). Human macrophages differentially produce specific resolvin or leukotriene signals that depend on bacterial pathogenicity. Nat. Commun. *9*, 59.

Zhou, Y., Cai, X., Loktinova, N.A., Wang, X., Nwokonko, R.M., Wang, X., Wang, Y., Rothberg, B.S., Trebak, M., and Gill, D.L. (2016). The STIM1-binding site nexus remotely controls Otrai1 channsl gating. Nat. Commun. *7*, 13725.

STAR★METHODS

KEY RESOURCES TABLE

REAGENT or RESOURCE	SOURCE	IDENTIFIER
Antibodies		
iNOS monoclonal antibody (CXNFT), alexa fluor 488, eBioscience™	Thermo Fisher Scientific	Cat# 53-5920-82, RRID:AB_2574423
NF-κB p65 (D14 × 10^{12}) XP rabbit mAb antibody	Cell Signaling Technology	Cat# 8242, RRID:AB_10859369
CD11b monoclonal antibody (M1/70.15)	Thermo Fisher Scientific	Cat# MA5-17857, RRID:AB_2539241
ORAI1 polyclonal antibody	Thermo Fisher Scientific	Cat# PA5-26378, RRID:AB_2543878
Anti-TRPC1 antibody	Alomone Labs	Cat# ACC-010, RRID:AB_2040234
Goat anti-rabbit IgG (H+L) secondary antibody, HRP	Thermo Fisher Scientific	Cat# 31460, RRID:AB_228341
STIM2 antibody	Cell Signaling Technology	Cat# 4917, RRID:AB_2198021
Anti-TRPC3 antibody produced in rabbit	Sigma-Aldrich	Cat# T5067, RRID:AB_261686
SAPK/JNK antibody	Cell Signaling Technology	Cat# 9252, RRID:AB_2250373
Rat Anti-CD16/CD32 monoclonal antibody, unconjugated, clone 2.4G2	BD Biosciences	Cat# 553142, RRID:AB_394657
Arginase 1 monoclonal antibody (A1exF5), PE-Cyanine7, eBioscience™	Thermo Fisher Scientific	Cat# 25-3697-82, RRID:AB_2734841
Phospho-STAT1 (Ser727) polyclonal antibody	Thermo Fisher Scientific	Cat# PA5-97355, RRID:AB_2809157
STAT1 monoclonal antibody (STAT1-79)	Thermo Fisher Scientific	Cat# AHO0832, RRID:AB_2536317
F4/80 monoclonal antibody (BM8), pacific blue	Thermo Fisher Scientific	Cat# MF48028, RRID:AB_10373419
CD80 (B7-1) monoclonal antibody (16-10A1), PE, eBioscience™	Thermo Fisher Scientific	Cat# 12-0801-82, RRID:AB_465752
CD68 antibody	Abcam	Cat# ab125212, RRID:AB_10975465
Anti-mouse IgG (H+L), F(ab) 2 fragment (alexa fluor 488 conjugate) antibody	Cell Signaling Technology	Cat# 4408, RRID:AB_10694704
Goat anti-rabbit IgG (H+L) highly cross-adsorbed secondary antibody, alexa fluor 488	Thermo Fisher Scientific	Cat# A-11034, RRID:AB_2576217
CD206 (MMR) monoclonal antibody (MR6F3), APC, eBioscience™	Thermo Fisher Scientific	Cat# 17-2061-82, RRID:AB_2637420
CD86 (B7-2) monoclonal antibody (GL1), PE, eBioscience™	Thermo Fisher Scientific	Cat# 12-0862-82, RRID:AB_465768
Chemicals, peptides, and recombinant proteins		
SKF96365	Abcam	Ab120280
Recombinant mouse interleukin-4 (IL-4)	Gibco	MAN004195
Mouse interferon-gamma (IFN-gamma)	eBioscience	BMS326
2-APB	Tocris Bioscience	524-95-8
Fludarabine	Tocris Bioscience	3495
Dihydrorhodamine	Sigma	D1054
Tetramethylrhodamine ethyl ester perchlorate (TMRE)	Sigma	87917
Tetramethylrhodamine	Sigma	87918
AS1517499	Selleckchem	S8685
Fura 2M	ThermoFisher	F1201
Critical commercial assays		
Phagocytosis assay kit (IgG FITC)	Cayman Chemical	500290
Cell proliferation kit I (MTT)	Sigma	11465007001

(*Continued on next page*)

Continued

REAGENT or RESOURCE	SOURCE	IDENTIFIER
NEBNext Ultra™ II RNA library prep kit for illumina		NEB #E7770
AbC total antibody compensation bead kit	Molecular probes	A10497
BrdU cell proliferation assay	Sigma	QIA58-200TEST
Seahorse XF cell Mito stress test kit	Agilent	103010-100
Experimental models: Organisms/strains		
Mouse: C57BL/6	The Jackson Laboratory	
Software and algorithms		
ImageJ	NIH	https://imagej.nih.gov/ij/
Image lab	Biorad	NA
FastQC v0.11.8	Babraham Bioinformatics	NA
FlowJo v10	FlowJo, LLC	NA
GraphPad prism v8.4.2	GraphPad LLC	NA
Origin v8	Origin LLC	NA
R/Bioconductor package cluster profiler v3.12.0	Bioconductor	NA

RESOURCE AVAILABILITY

Lead contact

Further information and requests should be directed by the Lead Contact, Brij B Singh (singhbb@uthscsa.edu).

Material availability

No unique materials were generated in this study.

Data code and availability

Data reported in this paper will be shared by the lead contact upon request.

This paper does not report original code.

Any additional information required to reanalyze the data reported in this paper is also available from the lead contact upon request.

EXPERIMENTAL MODELS AND SUBJECT DETAILS

Mice

For primary cells, femurs from C57BL/6 mice (6 weeks old, male), Orai1$^{fl/fl}$ (6 weeks old, male), and TRPC1$^{-/-}$ or Orai1$^{fl/fl}$ mice (6 weeks old, male) were used and bone marrow-derived macrophages (BMDMs) were isolated. The animal protocol has been approved by the institutional IACUC committee.

METHODS DETAILS

Primary macrophages, reagents, silencing and overexpression of Orai1 and TRPC1

Femurs were flushed out with PBS using a sterile needle, and BMDM cells were cultivated in DMEM medium (Life Technologies, Carlsbad, CA, USA) containing L929 conditioned media. After 5 days, BMDMs cells were then incubated at 37°C in DMEM medium supplemented with 10% FBS and 1% penicillin/streptomycin solution (Trouplin et al., 2013). Orai1 and TRPC1 adenovirus was purchased from AbmGood (Richmond, BC, Canada), and was amplified in HEK 293 using the manufacture's protocol. For overexpression experiments, 5 MOI of the virus encoding Orai1 or TRPC1 was added to 75% confluent cells. For silencing experiments respective Orai1siRNA (ThermoFisher, Assay ID: s99509) and TRPC1siRNA (ThermoFisher, Assay ID:104,443) was used, and the transfection was performed with Lipofectamine RNAi Reagent following the manufacture's protocol. Cells were seeded to be 70% confluent, and the Lipofectamine 2000 reagent was diluted in an optimal concentration (ThermoFisher, LMRNA015, 25 pmol per well in a

6-well dish) in Opti-MeM medium (Gibco, Dublin, Ireland). We added the lipofectamine to the diluted siRNA in a 1:1 ratio and incubated for 5 min at room temperature, after the stipulated time the complex was layered on the cells for 5 h followed by adding fresh media before using for individual experiments.

Cell proliferation assay

Cell proliferation were performed using Cell Proliferation ELISA, BrdU (colorimetric) kit from Roche (Basel, Switzerland). Cells are cultured in the presence of the respective test substances in a 96-well plate at 37°C for 24 hr. Subsequently, BrdU is added to the cells and the cells are re-incubated for 24 h. During this labeling period, the pyrimidine analogue BrdU is incorporated in place of thymidine into the DNA of proliferating cells. After removing the culture medium, the cells are fixed, and the DNA is denatured in one step by adding FixDenat. The immune complexes are detected by the subsequent substrate reaction. The reaction product is quantified by measuring the absorbance at the respective wavelength using spectrophotometer. The developed color and thereby the absorbance values directly correlate to the amount of DNA synthesis.

Cell viability assay

Cell viability was measured using 3-[4,5-dimethylthiazol-2-yl]-2,5-diphenyltetrasolium bromide (MTT) (Sigma-Aldrich, St Louis, MO, USA) according to the manufacturer's protocol. Cells were seeded in 96-well plates at a density of 0.5×10^5 cells/well and grown for 24 h. Cell viability was measured by using the MTT method. 10 μL of MTT reagent (5 mg/mL MTT in PBS) was added to each well and incubated in a CO2 incubator for 4 h. The resulting formazan dye was extracted with 100 μL of 0.01 N HCl in isopropanol, within an hour, measure the absorbance on an ELISA plate reader with a test wavelength of 570 nm and a reference wavelength of 630 nm. Cell viability was expressed as a percentage of the control culture.

Ca^{2+} measurement and electrophysiology

For fluorescence measurements, cells were incubated with 2 μM fura-2 (Molecular Probes, Eugene, OR, USA) for 45 min and then washed twice with Ca^{2+} free SES buffer. Cells were monitored with a CCD camera-based imaging system. The images of multiple cells collected at each excitation wavelength were processed using the C imaging, PCI software (Compix Inc., Cranberry, PA, USA), to provide ratios of Fura-2 fluorescence from excitation at 340 nm to that from excitation at 380 nm (F340/F380) as previously described (Singh et al., 2000; Sun et al., 2014). For patch-clamp experiments, coverslips with cells were transferred to the recording chamber and perfused with an external Ringer's solution of the following composition (mM): NaCl, 145; KCl, 5; $MgCl_2$, 10; $CaCl_2$, 1; HEPES, 10; Glucose, 10; pH 7.4 (NaOH). The patch pipette had resistances between 3 and 5 m after filling with the standard intracellular solution that contained the following (mM): cesium methanesulfonate, 145; NaCl, 8; $MgCl_2$, 10; HEPES, 10; EGTA/BAPTA, 10; pH 7.2 (CsOH). The maximum peak currents were calculated at a holding potential of −80 mV. The I/V curves were made using a ramp protocol where current density was evaluated at various membrane potentials and plotted.

RNA isolation, RNA seq, and quantitative Real-Time PCR (RT-PCR) analysis

Total RNA from BMDMs stimulated with medium alone (NS), or in the presence of IFNγ at 20 ng/mL and IL4 at 20 ng/mL for different time points (2 h, 6 h, and 24 h) were isolated using RNeasy Mini kit (Qiagen #74104) using manufacturers' instructions. One microgram of total RNA from each sample was reverse transcribed into cDNA by using a high capacity cDNA reverse transcription kit according to the manufacturers' instructions (Applied Biosystems, CA, USA). Transcript levels of TRPC1 and Orai1 or the housekeeping ribosomal 18 S, were PCR amplified in each sample by using specific primers. Sequences of the specific primers used for 18 S, TRPC1 and Orai1 are as follows: 18 S (sense) 5′-CATGTGGTGTTGAGG AAAGCA-3′ and (antisense) 5′-GTCGTGGGTTCTGCATGATG-3′; TRPC1 (sense) 5′-CGTAGATGTGCTTGGGAGAAA-3′ and (antisense) 5′-CCCACTACTTCAGAGTCGATTG-3′ and Orai1 (sense) 5′-CTGGCGCAAGCTCTACTTA-3′ and (antisense) 5′-GACTTCCACCATCGCTACC-3′. TRPC1 and Orai1 mRNA levels were normalized to the mRNA level of the housekeeping gene 18S in the same sample. The fold change was calculated by dividing the normalized value of the gene of interest in stimulated samples with the corresponding normalized value in unstimulated samples. Similarly, total RNA was isolated from bone marrow derived macrophage of age-matched wild type and $TRPC1^{-/-}$ mice. Quality of RNA was analyzed using Bioanalyzer (Agilent Technologies), and RNA Integrity Number greater than seven were used for RNA-Seq library preparation using NEBNext Ultra II RNA Library Prep Kit for Illumina (NEB, #E7770) as per the manufacturer's instruction. The

library was sequenced in the HiSeqX instrument, and approximately 40 million, 150 bp paired-end reads were generated for each sample. Sequencing quality control for reads was performed with FastQC v0.11.8. Based on the FastqC report, adapters were trimmed using Trimmomatic v0.39 and reads were aligned to a human genome (mm 10) using STAR v2.7.1a. Differential expression analyses for control and TRPC1$^{-/-}$ samples were performed using the R/Bioconductor package DESeq2 v1.24.0. Genes were considered differentially expressed if they had an FDR (pAdj value) of 0.05 or less. Gene ontology and KEGG pathway enrichment analyses were performed using the R/Bioconductor package clusterProfiler v3.12.0.

CHIP assays and confocal microscopy

Macrophages were seeded into 15-cm dishes, pulsed with medium alone (NS), or in the presence of IFNγ at 20 ng/mL, or IL4 at 20 ng/mL for 2, 6 and 24 hrs at 37°C. Cells were cross-linked with formaldehyde for 10 min at room temperature, followed by addition of 125 mM glycine for 5 min at 4°C. Cells were washed in ice-cold PBS and harvested. Cells were lysed by sonication to generate 250- to 150-bp DNA fragments using Covaris Sonicater. Immunoprecipitation was performed with the antibodies indicated anti-pNFKβ (Santa Cruz Biotechnology, sc-8008X), anti-pStat1 (Santa Cruz Biotechnology, sc-8394X), anti-pStat6 (Cell signaling, 56554S), anti-STAT3 (Cell signaling, cat number: 9145S), Anti-IRF-4 (Santa Cruz Biotechnology, sc-48338), Anti-PPARγ (Santa Cruz Biotechnology, sc-7273), and IgG (Abcam, ab 171,870) was used as a control. Precipitated DNAs were detected by polymerase chain reaction (PCR) using specific primers. Sequences for TRPC1 Promotor were (sense) 5′-TTATCCGCTGCCTGTTTGT-3′; antisense 5′-TGCTTTGGCCAGGCTTTA-3′. Real-time PCR analysis on respective immuno-precipitated DNA was performed using SYBR green as the detection dye. The percent input for each sample was calculated based on a standard curve using 10%, 1%, 0.1%, and 0.01% of input DNA. Precipitated DNA with anti-IgG served as a background control. For confocal microscopy, individual cells were plated on glass coverslips, stained with individual antibodies, and imaged at 40× objective using Zeiss confocal system.

Protein extractions and western blotting

Protein lysates were prepared in lysis buffer (10 mM Tris,140 mMNaCl,1%NP-40, 0.5% SDS, and protease inhibitors, pH 8.0), protein concentrations were determined, using the Bradford reagent (Bio-Rad Laboratories, Hercules, CA, USA), and 25–50 ug of proteins were resolved on NuPAGE Novex 4–12% BisTris gels, transferred to PVDF membranes The membrane was blocked with skim milk in PBST solution and incubated with primary antibodies. After washing with PBST, secondary antibodies were applied and detected by the Clarity Max Western ECL Substrate (Bio-Rad Laboratories, Hercules, CA, USA). Densitometric analysis was performed using ImageJ analysis and results were corrected for protein loading by normalization for β-actin (Cell Signaling, 4970S) as previously described (Singh et al., 2004). Blot stripping was performed whenever necessary, using Restore PLUS Western Blot Stripping Buffer (Thermo Fisher, Waltham, MA, USA). The blots were washed with PBS Tween 20 (Sigma, St. Louis, MO, USA), then immersed in stripping buffer for 15mins at room temperature, washed again and blocked for another 30 min before incubation with the new antibody. The following primary antibodies (dilution accordingly by manufacturer's protocol) were used for Western blot analysis: anti-STIM1 (Cell Signaling, D88E10), anti-Orai1 (Thermo-Fisher, PA5-26378), anti-Orai2 (Abcam, ab180146), anti-Orai3 (Abcam, ab254260), anti-TRPC1 (Alamone, ACC-010), anti-TRPC3 (ThermoFisher, PA577307), anti-STIM1 (Cell Signaling, 5668S), anti-STIM2 (Cell Signaling, 4917S), anti-JNK (Cell Signaling, 9252), anti-pJNK (Thr81) (Cell Signaling, 2676), anti-NFκB (p65) (Cell Signaling, 8242S), anti-pNFκB p65 (pp65) (Cell Signaling, 3033S), anti-STAT1 (Cell Signaling, 14994S), anti-pSTAT1 (Cell Signaling, 9167S), anti-STAT6 (Cell Signaling, 5397S), anti-pSTAT6 (Cell Signaling, 56554S), anti-iNOS (Cell Signaling, 13120S), anti-Arginase 1 (Cell Signaling, 93668S), Goat anti-rabbit (Cell Signaling, 7074S) and goat anti-mouse (Cell Signaling, 7076S) IgGs were used as secondary antibodies.

Measurement of cytokines levels

IL-6, TNF-α, and IL-1β levels in the supernatant were measured using the Enzyme-Linked ImmunoSorbent Assay (ELISA) kit (Life Technologies, Carlsbad, CA, USA) following the manufacturer's instructions using standard diluent buffers designed for use with mouse serum. We use Lipopolysaccharides (LPS 100 ng/mL, Sigma, St. Louis, MO, USA) as a positive control, cells were incubated for 3hrs after treatments. HMGB1, Histone 3 and hsp70 levels were measured by direct Elisa by self-coating protocol, previously described. All samples were measured on a single 96-well plate for each cytokine, the cultured medium was centrifuged at 800 G at for 5 min 4°C and the supernatant was used as the sample. Based on that

criterion, all cytokine values for the murine cell line Raw 264.7 and bone marrow-derived macrophages serum samples examined were above the limit of detection and within the reportable range of each assay.

Macrophage polarization and STAT inhibition

BMDM was exposed to IFNγ (20 ng/mL, Peprotech, Rocky Hill, NJ, USA) to generate the M1 phenotype, and IL4 (20 ng/mL, Peprotech, Rocky Hill, NJ, USA) to generate M2 phenotype. Stimulated cells were removed from wells and incubated in anti-mouse BD Fc Block CD16/CD32 (BD Biosciences, San Jose, CA) for 30 min on ice in FACS buffer (PBS with 3% FBS), then surface stained with antibodies for anti-iNOS conjugated with PE (Cell Signaling, D6B6S) and Arginase-1 (Cell Signaling, D43EM), CD80 (Abcam, Cambridge, UK) and CD206 (Abcam, Cambridge, UK) for 15 min at 4°C. Cells were washed three times with FACS buffer, then fixed with paraformaldehyde (4%) for 40 min at 4°C and washed three times in PBS. For intracellular staining, cells were permeabilized by adding ice-cold 100% methanol slowly to the cold cells, while gentle vortexing to a final concentration of 90% methanol. Cells were then incubated for 30 min at 4°C prior to staining with primary antibody anti-Arginase for 1 h at 4°C, cell were then washed 3× by centrifugation at 400 g for 5 min with FACS buffer and then incubated in the dark with conjugate antibody (Abcam, Cambridge, MA, USA) at optimal dilution (according to the manufacturer's instructions) for 30 min at 4°C. Cells were then washed 3× by centrifugation at 400 g for 5 min, then analyzed by LSRII (BD Biosciences, San Jose, USA) and FlowJo software version 9.0. Following polarization, fludarabine (5 μM; Selleck Chemicals, Shanghai, China) or AS1517499 (100 mM, Selleck Chemicals, Shanghai, China); was added, and cells were cultured for 24 h prior to being analyzed by western blotting and flow cytometer analysis.

Flow cytometry

On day 7, formation of mature BMDM is evaluated using flow cytometry analysis and fluorophore conjugated antibodies. Cells were resuspended with FACS buffer (PBS supplemented with 0.2% BSA), then blocked with Anti-Mouse CD16/CD32 Fc Blocker (BD Pharmigen, San Jose, CA, USA) for 15 min. After blocking, cells were tested for the expression of Anti-CD11b antibody [M1/70] (PE/Cy5) (Abcam, Burlingame, CA, USA) and F4/80 Monoclonal Antibody (BM8), Pacific Blue (Thermo Fisher, Waltham, MA, USA) for macrophage line confirmation. For M1 macrophages, cells were stained with Anti-Mouse CD80 PE (eBioscience, San Diego, CA, USA) and Anti-Mouse iNOS Alexa Fluor 488 (eBioscience, San Diego, CA, USA); for M2 macrophage cells were stained with Anti-Mouse Arginase 1 PE-Cyanine (eBioscience, San Diego, CA, USA) and Anti-Mouse CD206 APC (eBioscience, San Diego, CA, USA). Cells were incubated for for 30 min at 4°C, then quantified on a BD LSR II (BD Pharmigen, San Jose, CA, USA).

Phagocytosis assay

Cells were assessed for phagocytic activity using the Phagocytosis Assay Kit (Cayman Chemical, Ann Arbor, MI, USA). Cells were incubated with latex beads with rabbit IgG-FITC conjugates (1:100) for 4 h followed by a 15-min incubation with Hoechst (ThermoFisher, Waltham, MA) to quench non-phagocytosed bead fluorescence. For the flow cytometer part of the assay, after incubation cells were washed and analyzed by BD LSRII. The phagocytic index was calculated following the formula: phagocytic index = (number of engulfed cells/number of macrophages) × (number of macrophages containing engulfed cells/total number of counted macrophages) × 100.

Measurement of mitochondrial oxygen consumption rate

Bone Marrow Derived Macrophages (BMDM) from WT and Orai1$^{fl/fl}$ mice (n = 3) were plated on 96 well Agilent Seahorse XF Cell culture microplates at a density of 4 × 10^5 cells per well. The macrophages were plated in their normal growth media overnight. The plated Orai1$^{fl/fl}$ macrophages were infected with Adeno-Cre virus (Ad) mediated Cre deletion for floxed sequences (20 MOI) for 72 h. After 48 h of Cre virus infection, naive macrophages (M0) from WT and Orai1$^{fl/fl}$ mice were polarized to become pro-inflammatory macrophages (M1) and anti-inflammatory macrophages (M2) upon Interferon-γ (IFNγ) or interleukin-4 (IL-4) stimulation for 24 h. After polarization, the media was changed to Seahorse XF Cell Mito Stress Test Kit (Agilent) assay media supplemented with glucose, glutamine, pyruvate concentrations equivalent to that of the growth media. naive Mφ, M1 and M2 macrophages were treated with the SOCE channel inhibitor, 2ABP (50 μM) for 15 min and oxygen consumption rate (OCR) was measured at 37°C in an XF96 extracellular flux analyzer (Seahorse Bioscience, Agilent), which had been previously calibrated using Seahorse XF Calibrant solution (Seahorse Bioscience, Agilent) in a CO_2-free incubator overnight. Respiratory chain inhibitors were then loaded into the XF96 flux analyzer and added sequentially to cells

at indicated time points. M0, M1 and M2 macrophages received oligomycin (2 μM), FCCP (5 μM), and a mixture of antimycin A and rotenone (1 μM) sequentially. Data were collected using Agilent Seahorse Wave 2.6.1 Desktop software and exported to GraphPad Prism version 8 for analysis.

Measurement of mitochondrial morphology and membrane potential

BMDM from Orai1$^{fl/fl}$ mice were plated on 35 mm MatTek dishes, in normal growth media. The plated Orai1$^{fl/fl}$ macrophages were infected with adeno-Cre virus (20 MOI) and after 48 h of Cre virus infection, naive macrophages (M0) from WT and Orai1$^{fl/fl}$ mice were polarized to become pro-inflammatory macrophages (M1) and anti-inflammatory macrophages (M2) upon IFNγ or IL-4 stimulation for 24 h. The mitochondrial morphology and the $\Delta\Psi_m$ were determined after staining with dihydrorhodamine 123 (2.5 μM) (ex/em 505/524 nm) and Tetramethylrhodamine, ethyl ester, perchlorate (TMRE; 100 nM; ex/em 556/610 nm) at room temperature) for 30 min. The stained macrophages were washed and imaged using Leica SP8 Confocal microscope (Manheim, Germany) coupled with a temperature-controlled environmental chamber. The images were acquired, and mitochondrial length, area and perimeter were quantified using the Leica Application Suite X software and analyzed using GraphPad Prism version 8.

QUANTIFICATION AND STATISTICAL ANALYSIS

Data analysis was performed using a one-way ANOVA or Student *t*-test on Graphpad prism 8.0. Ca^{2+} measurement and electrophysiology were analyzed using Origin 9.0. Experimental values are expressed as means ± SD. * indicates significance of $P < 0.05$, ** of $P < 0.01$ and *** of $P < 0.001$, respectively.